Available online at www.sciencedirect.com
ScienceDirect
Journal of Computational Physics 223 (2007) 208–234
JOURNAL OF COMPUTATIONAL PHYSICS
www.elsevier.com/locate/jcp

An asymptotic preserving scheme for the two-fluid Euler–Poisson model in the quasineutral limit

Pierre Crispel [a,b,c], Pierre Degond [c], Marie-Hélène Vignal [c,*]

[a] CNES Centre de Toulouse, 18 av. Ed. Belin, 31401 Toulouse cedex 4, France
[b] ONERA Centre de Toulouse, 2 av. Ed. Belin, 31055 Toulouse cedex 4, France
[c] MIP, Univ. P. Sabatier, 118 rte de Narbonne, 31062 Toulouse cedex 4, France

Received 17 January 2006; received in revised form 26 June 2006; accepted 10 September 2006
Available online 25 October 2006

Abstract

This paper deals with the modeling of a plasma in the quasineutral limit using the two-fluid Euler–Poisson system. In this limit, explicit numerical schemes suffer from severe numerical constraints related to the small Debye length and large plasma frequency. Here, we propose an implicit scheme which reduces to a scheme for the quasineutral Euler model in the quasineutral limit. Such a property is referred to as ''asymptotic preservation''. One of the distinctive features of this scheme is that it has a comparable numerical cost to that of an explicit scheme: simply the Poisson equation is replaced by a different (but formally equivalent) elliptic problem. We present numerical simulations for two different one-dimensional test-cases. They confirm the expected stability of the scheme in the quasineutral limit. They also show that this scheme has some accuracy problems in the limit of small electron to ion mass ratio in reproducing the correct electron velocity. But this problem is already present in the results of the classical algorithm. Numerical simulations are also performed for a two-dimensional problem of a plasma expansion in vacuum between two electrodes.

Keywords: Asymptotic preserving scheme; Quasineutral limit; Explicit cost; Euler–Poisson; Plasma

1. Introduction

In this paper, which has been summarized in the short note [14], we are interested in numerical algorithms to solve plasma fluid models. For the sake of simplicity, we assume that the plasma consists of electrons and one ion species and the model consists of the isentropic Euler equations for each species coupled with the Poisson equation. The methodology can actually be extended to other types of fluid models, such as full Euler equations for both species, of Euler equations for the ions and drift-diffusion equations (supplemented by an energy equation) for the electrons like in [9,17].

* Corresponding author. Tel.: +33 5 61 55 69 22; fax: +33 5 61 55 83 85.
E-mail addresses: crispel@mip.ups-tlse.fr (P. Crispel), degond@mip.ups-tlse.fr (P. Degond), mhvignal@mip.ups-tlse.fr (M.-H. Vignal).

0021-9991/$ - see front matter
doi:10.1016/j.jcp.2006.09.004

There are two important physical length and time scales associated with this model (see e.g. [5,43]): the Debye length and the electron plasma period. The Debye length measures the typical length scale of charge imbalances in the plasma, and the electron plasma period is the period of the oscillations which take place (due to the electrostatic restoring force) when such charge imbalances occur. We are interested in situations where both parameters can be very small compared with typical macroscopic length and time scales. In this so-called quasineutral regime, the local electric charge vanishes everywhere. However, simultaneously, the electron plasma period becomes very small as well, so that when charge imbalances accidentally occur (as a numerical artifact for instance), very high frequency plasma oscillations are triggered. When a standard explicit scheme is used, these micro-scale phenomena must be resolved. Hence, the space and time steps must be smaller than the Debye length and electron plasma period otherwise a numerical instability is generated. The satisfaction of these constraints requires huge computational resources which make the use of explicit methods almost impracticable.

The search for schemes free of such constraints has been the subject of a vast literature. A number of works deal with particle models (instead of fluid models). Basically, two kinds of implicit methods have been proposed for Particle-in-Cell (PIC) simulations: the direct implicit method [8,45] and the implicit moment method [50,51]. Both method have then been coupled with the Maxwell equations ([3,35,44] for the direct implicit method [52,53,73] for the implicit moment method and [31,32] for the use of the Darwin approximation of the Maxwell system). For collisional kinetic models, or hybrid (electron) fluid–(ion) kinetic models, we can refer to [57,58]. There has been an intense literature on this subject and it is virtually impossible to cite it all. These methods have proved extremely efficient in number of situations but there are still regions where short time steps must be used (see e.g. the recent discussion in [30]). Sophisticated numerical algorithms have been developed to overcome this problem, such as multiscale simulations [29], or recently, Discrete Event Simulation techniques [40], but their implementation requires specific developments. So the improvement of classical time-stepping strategies, if possible, would offer attractive perspectives.

Our work is in this direction but (so far) deals with fluid models. For fluid models the literature is comparatively less abundant. We can refer to the pioneering work [27], and more recently to [7,9,62,64]. When the fluid models are drift-diffusion models, implicit strategies have been proposed in [71,72,46].

To cancel the fast scales associated with electron plasma frequency, quasineutral models have been very frequently considered [25]. Most frequently, hybrid (electron) fluid–(ion) kinetic quasineutral models have been considered [36,48,59] but other cases have also been investigated [39,47]. Recently, two-fluid quasineutral models have been studied [13,15,18–21]. Such models are formally obtained by letting the ratio of the Debye length to the macroscopic length scale and accordingly that of the electron plasma period to the macroscopic time scale to zero.

However, in situations where quasineutral and non-quasineutral regions coexist, a specific treatment is needed to connect the quasineutral model with a non-quasineutral model across the interface. Such situations arise in sheath problems [28,34,65–68], ion extraction problems [37], plasma diode modeling [69], arc formation on satellite solar cells [2,4,6,24] and potentially many other situations where edge plasmas occur, like the divertor region of a tokamak [42].

In such problems, one has often to deal with a dynamic interface the tracking of which gives rise to a complex numerical problem. Various algorithms have been proposed for interface dynamics, such as Front Tracking [70], Volume of Fluid methods [78], Level Set methods (see e.g. [55,63]) or Diffuse Interface Methods (see e.g. [1,61]). Specific algorithms have been developed in the context of PIC simulations of plasmas [75]. All these methods require specific developments. Additionally, the interface dynamics is not a priori known, and must either be derived from an asymptotic analysis like in [19,20], or [34], or must be inferred from physical considerations. In both cases, great care is required to ensure that the proper dynamics is implemented. Another problem is related to the fact that the quasineutral to non-quasineutral transition may not be a sharp transition, but rather a fairly diffuse one, and its approximation into a sharp interface may actually lead to some unphysical behavior.

For these reasons, it is highly desirable to develop numerical methods which automatically shift from a quasineutral to a non-quasineutral model across the transition region when such a transition is encountered. In this work, we show that the two-fluid Euler–Poisson model can be discretized by means of an implicit scheme such that, in the quasineutral limit, a discretization of the quasineutral Euler model is recovered. Such

a property is sometimes referred to as ''asymptotic preservation'' (in that the scheme preserves the asymptotic limit) and the scheme then enjoys the so-called AP property (asymptotic preserving).[1] Other approaches targeting the same property have been previously published in the literature, such as [7,9].

Our strategy does not require any restrictive assumption on the solution of the problem and is valid in any number of space dimensions. Additionally, in spite of being implicit, the scheme has the same computational cost as the standard explicit strategy, the resolution of the Poisson equation being replaced by that of a different (but formally equivalent) elliptic equation, which is not more difficult to solve. This is, up to our knowledge, the first time that this elliptic equation is introduced. In this paper, we report on numerical simulations in one and two space dimensions which experimentally prove that the scheme performs well in the quasineutral limit. In a forthcoming work by the same authors in collaboration with Liu, a linearized stability analysis of the scheme is performed. It demonstrates that its stability region is independent of the Debye length and of the electron plasma period.

To better introduce our strategy, we first consider the continuous model and show that the Poisson equation can be reformulated into an elliptic equation which does not degenerate when the Debye length and electron plasma period tend to zero (like the Poisson equation does), but instead leads to the equation for the quasineutral potential. This is done in Section 2.

Then, in Section 3, we propose an implicit time-stepping strategy which allows to reproduce the derivation of the reformulated elliptic equation for the potential in a discrete setting. Again, the reformulated equation does not degenerate when the Debye length and electron plasma period tend to zero but instead leads to the equation for the quasineutral potential. This indeed means that the scheme enjoys the (AP) property. An important point is that we can formulate this time-stepping strategy in such a way that the (AP) scheme has a comparable cost to that of an explicit discretization.

The standard time-stepping strategy (following [27]; see also [64]) already involves implicit electric force terms in the momentum balance equations. Our implicit time-stepping strategy requires that, additionally to the electric force terms, the mass flux terms in the mass conservation equations be taken implicitly. By contrast, the momentum flux terms (both the drift and pressure ones) can be discretized explicitly. By taking these terms explicitly, we may formulate the algorithm in such a way that the (AP) scheme has a comparable cost to that of the standard time-stepping strategy. Time-implicit algorithms for the compressible Euler equations have been considered in many references, see e.g. [10,76,77].

With some of the hydrodynamic fluxes discretized explicitly, the stability domain of the scheme is still limited by the CFL number of the hydrodynamics. This can be quite detrimental for electrons because of their very small mass. However, the time-stepping strategy can be extended in order to waive the limitation due to the very small electron mass. This improvement will be reported in future work. The small electron mass problem is somewhat similar to the low Mach number limit in compressible flows (see e.g. [41]).

Finally, space-discretization strategies are discussed. Since we are interested in stiff problems where the plasma density drops to virtually zero, we have considered a modified Lax–Friedrichs scheme, which is very robust. Obviously, this is a very diffusive scheme and the control of numerical diffusion requires further improvements. There is a huge variety of hydrodynamic solvers which require a systematic testing for determining the best (AP) coupled strategy with the Poisson equation. As a preliminary step, we have investigated two other solvers, the Lax–Wendroff scheme and a Riemann solver based scheme, the Polynomial scheme [15,22]. They both perform well in smooth regions (as can be seen in Section 4) but develop instabilities at the plasma–vacuum transition. Still, the results with the modified Lax–Friedrichs scheme already seem promising, as Section 4 will show.

Indeed, Section 4 is devoted to the discussion of the numerical results. First, comparisons between the classical and (AP) schemes are provided in a one-dimensional geometry. The first test problem consists of a periodic perturbation of a quasineutral uniform stationary plasma with non-zero current. For this test-case, an exact solution of the linearized Euler system about the considered steady state is analytically known. For small perturbations, the solutions of the linearized and nonlinear problems are believed to be close. The classical and

[1] This terminology has been introduced by S. Jin for relaxation limits of kinetic systems [38].

asymptotic preserving scheme are compared. We numerically observe that the (AP) scheme remains stable while the classical scheme develops instabilities for time steps greater than the electron plasma period.

The second configuration is a one-dimensional physical application linked to high-current plasma diodes [18–21,69] and arcing on satellite solar cells [4,6,15,24]. This test-case describes the expansion of a quasineutral plasma in the vacuum separating two electrodes. The high density quasineutral plasma is emitted at the cathode and undergoes a thermal expansion. At the plasma–vacuum interface, electron emission occurs in the Child–Langmuir regime (see e.g. [5,16,23]). This test-case is particularly well adapted to the (AP) scheme, since a transition between a quasineutral region (the plasma) to a non-quasineutral one (the gap where the electrons are accelerated) occurs. We observe that the (AP) scheme remains stable in all the cases while the classical scheme develops a non-physical behavior for time steps greater than the plasma electron period.

Finally a two-dimensional simulation is presented. The physical problem is again that of the plasma expansion between two electrodes. The results show that the scheme performs well in a multi-dimensional setting, and confirms its stability for large time and space steps (compared to the Debye length and the electron plasma period). Such a simulation would be virtually impossible to achieve with an explicit scheme, and would require considerable computer resources.

2. The two-fluid Euler–Poisson system and its quasineutral limit

In this section, we present the two-fluid Euler–Poisson system and its quasineutral limit. We review the fundamental time and length scales (the electron plasma period and the Debye length). We show that the Poisson equation can be reformulated into an elliptic equation which does not degenerate in the quasineutral limit and, in this limit, provides the equation for the quasineutral potential.

2.1. The two-fluid isentropic Euler–Poisson system

We consider a plasma constituted of electrons and one positively charged ion species. We denote by $m_{i,e}$ the ion and electron masses, by $n_{i,e}$ their densities and by $u_{i,e}$ their mean velocities. For simplicity, the ions are supposed singly charged and both the electron and ion pressure laws, $p_{i,e}$, are assumed isentropic, i.e. $p_{i,e} = c_{i,e} n_{i,e}^{\gamma_{i,e}}$, where $\gamma_{i,e} > 1$ are the ratio of specific heats and $c_{i,e} > 0$ are given positive constants. We denote by ϕ the electric potential.

We suppose that the position variable x belongs to the physical domain $\Omega \subset \mathbb{R}^d$, $d = 1$, 2, or 3. We shall discard the description of the boundary conditions (but some of them are treated in the numerical examples below). The two-fluid Euler–Poisson system in the domain Ω is written

$$\partial_t n_i + \nabla \cdot (n_i u_i) = 0, \tag{1}$$

$$m_i[\partial_t(n_i u_i) + \nabla \cdot (n_i u_i \otimes u_i)] + \nabla p_i(n_i) = -e n_i \nabla \phi, \tag{2}$$

$$\partial_t n_e + \nabla \cdot (n_e u_e) = 0, \tag{3}$$

$$m_e[\partial_t(n_e u_e) + \nabla \cdot (n_e u_e \otimes u_e)] + \nabla p_e(n_e) = e n_e \nabla \phi, \tag{4}$$

where e is the positive elementary charge and where the electric field $E = -\nabla\phi$ is given by the Poisson equation

$$-\varepsilon_0 \Delta \phi = e(n_i - n_e), \tag{5}$$

with ε_0 the vacuum permittivity.

Let us point out that our strategy can easily be extended to more complex models. We can consider full Euler systems with energy equations, multiple ion species (including negatively charged ions). Similarly, we could consider that some or all species are rather modeled by drift-diffusion equations (possibly supplemented by energy equations). Finally, the Maxwell equations can be substituted to the Poisson equation as well. All these points will be developed in future work. The consideration of kinetic models instead of fluid ones is under investigation.

The two important physical scales which characterize this model (see [5,43]) are the Debye length λ_D and the electron plasma frequency ω_p given by

$$\lambda_D = \left(\frac{\varepsilon_0 k_B T_0}{e^2 n_0}\right)^{1/2}, \quad \omega_p = \left(\frac{n_0 e^2}{\varepsilon_0 m_e}\right)^{1/2},$$

where k_B is the Boltzmann constant, n_0 is the density scale ($n_0 \sim n_i \sim n_e$), T_0 is the temperature scale ($k_B T_0 \sim p_i(n_0)/n_0 \sim p_e(n_0)/n_0$) and m_e is the electron mass. The Debye length measures the typical length scale of charge imbalances in the plasma, and the electron plasma period is the period of the oscillations which take place (due to the electrostatic restoring force) when such charge imbalances occur. We note that an ion plasma frequency can be defined (changing m_e into m_i) but, due to the large ion to electron mass ratio, this parameter is much smaller than ω_p. The electron plasma period is defined by $\tau_p = 1/\omega_p$.

We are interested in the very frequent situation where both the Debye length and the electron plasma period are very small compared with typical macroscopic length and time scales. In this so-called quasineutral regime, the local electric charge vanishes everywhere. However, simultaneously, the electron plasma period becomes very small as well, so that when charge imbalances accidentally occur (as a numerical artifact for instance), very high frequency plasma oscillations are triggered.

When a standard explicit scheme is used, these micro-scale phenomena must be resolved. Hence, the space and time steps Δx and Δt, must satisfy

$$\Delta x \leqslant \lambda_D \quad \text{and} \quad \omega_p \Delta t \leqslant 1,$$

otherwise a numerical instability is generated. These constraints are particularly penalizing in quasineutral regimes and simulations require huge computational resources. For this reason, the quasineutral model is usually preferred.

To introduce the quasineutral model, it is convenient to first perform a scaling of the Euler–Poisson problem. The scaled variables are given by $\bar{x} = x/L$ and $\bar{t} = tu_0/L$ where L is the typical length of the problem and u_0 is the ion velocity scale (typically $u_0 = (k_B T_0/m_i)^{1/2} = (p_i(n_0)/(n_0 m_i))^{1/2}$, where we recall that n_0 and T_0 are the density and temperature scales). The scaled unknowns are defined by $\bar{n}_i = n_i/n_0$, $\bar{n}_e = n_e/n_0$, $\bar{u}_i = u_i/u_0$, $\bar{u}_e = u_e/u_0$, $\bar{\phi} = e\phi/(m_i u_0^2)$ and $\bar{p}_{i,e} = p_{i,e}/(m_i n_0 u_0^2)$. Inserting this scaling into (1)–(4) and omitting the bars gives rise to the following scaled two-fluid Euler–Poisson model:

$$\partial_t n_i + \nabla \cdot (n_i u_i) = 0, \tag{6}$$

$$\partial_t (n_i u_i) + \nabla f_i = -n_i \nabla \phi, \tag{7}$$

$$\partial_t n_e + \nabla \cdot (n_e u_e) = 0, \tag{8}$$

$$\partial_t (n_e u_e) + \nabla f_e = n_e \nabla \phi / \varepsilon, \tag{9}$$

$$-\lambda^2 \Delta \phi = n_i - n_e, \tag{10}$$

where f_i and f_e are the scaled momentum fluxes:

$$f_i = n_i u_i \otimes u_i + p_i(n_i)\mathrm{Id} \quad \text{and} \quad f_e = n_e u_e \otimes u_e + \frac{1}{\varepsilon} p_e(n_e)\mathrm{Id}, \tag{11}$$

with $\epsilon = m_e/m_i$ being the particle mass ratio and the symbols $\otimes$ and Id respectively denoting the tensor product of vectors and the Identity tensor. The terms ∇f_i, ∇f_e denote the divergence of the tensors f_e and f_i.

The mathematical theory of the Euler–Poisson system has been investigated in [12,56] for the isothermal case and in [49] for the isentropic case.

The parameter λ is the scaled Debye length given by $\lambda = \lambda_D/L$. Note that the scaled plasma frequency is given by $\omega = \omega_p L/u_0 = 1/(\sqrt{\epsilon}\lambda)$. In what follows, we shall keep ε an order O(1) quantity and investigate the limit $\lambda \to 0$. However, the strategy can be extended when both parameters λ and ε tend to zero. This will be reported in future work. Note that the limit $\varepsilon \to 0$ alone is similar to the so-called low Mach number limit of hydrodynamics (see e.g. [41]).

2.2. The quasineutral model

The formal quasineutral limit on the two-fluid Euler–Poisson system $\lambda \to 0$ has been studied in a series of works [20,15]. Here, we recall some results included in these works.

Formally passing to the limit $\lambda \to 0$ in the two-fluid Euler–Poisson problem merely amounts to replacing Eq. (10) by the quasineutrality constraint $n_i = n_e$. The Poisson equation is lost, while the electrostatic potential becomes the Lagrange multiplier of this constraint. Assuming that quasineutrality is satisfied initially $n_i(t=0) = n_e(t=0)$ (the possible occurrence of non-quasineutral initial layers being discarded in these considerations), the constraint $n_i = n_e$ can be expressed by taking the difference of the mass conservation equations (6), (8) and leads to the divergence-free constraint for the scaled electric current $j = n_i u_i - n_e u_e$:

$$\nabla \cdot j = \nabla \cdot (n_i u_i - n_e u_e) = 0. \tag{12}$$

Now, taking the divergence of Eqs. (7) and (9), subtracting them and inserting into (12), we obtain the following elliptic equation for the quasineutral potential ϕ:

$$-\nabla \cdot \left(\left(n_i + \frac{n_e}{\epsilon} \right) \nabla \phi \right) = \nabla^2 : (f_i - f_e),$$

where the symbols ∇^2 and respectively denote the tensor of second order derivatives and the contracted product of two tensors.

In summary, the quasineutral model consists of the following system:

$$\partial_t n_i + \nabla \cdot (n_i u_i) = 0, \tag{13}$$

$$\partial_t (n_i u_i) + \nabla f_i = -n_i \nabla \phi, \tag{14}$$

$$\partial_t n_e + \nabla \cdot (n_e u_e) = 0, \tag{15}$$

$$\partial_t (n_e u_e) + \nabla f_e = n_e \nabla \phi / \varepsilon, \tag{16}$$

$$-\nabla \cdot \left(\left(n_i + \frac{n_e}{\epsilon} \right) \nabla \phi \right) = \nabla^2 : (f_i - f_e). \tag{17}$$

Again, this model is formally equivalent with taking the quasineutrality limit $n_i = n_e$ of the Euler–Poisson problem, provided that quasineutrality is satisfied initially.

Quasineutral limits have been rigorously studied in [11,74,67] for simplified systems.

We first note that the two-fluid Euler–Poisson system (6)–(10) and the quasineutral Euler system (13)–(17) only differ by the elliptic equations for the potential ϕ namely the Poisson equation (10) for the former, and the quasineutral equation (17) for the latter. The second remark is that these two equations are quite different, explaining why the two regimes have so different properties. The third remark is that there is no direct way of guessing Eq. (17) from the quasineutral limit of (10). However, if we wish to attempt to find a unified numerical strategy for both regimes, we need to find an equation which embeds both (10) and (17). In the next section we present a way of unifying these two different equations.

2.3. A reformulation of the Poisson equation

Here we return to the Euler–Poisson system and provide a formally equivalent formulation to the Poisson equation (10) which allows to recover the quasineutral equation (17) in the quasineutral limit. We show that the Poisson equation is formally equivalent to the following:

$$\varepsilon \lambda^2 \partial_{tt}^2 (-\Delta \phi) - \nabla \cdot ((\epsilon n_i + n_e) \nabla \phi) = \epsilon \nabla^2 : (f_i - f_e), \tag{18}$$

provided that

(i) f_i and f_e are the fluxes of the Euler system (11),
(ii) initially, the Poisson equation is satisfied:

$$(-\lambda^2 \Delta \phi - \rho)_{t=0} = 0 \quad \text{and} \quad \left(\frac{\mathrm{d}}{\mathrm{d}t} (-\lambda^2 \Delta \phi - \rho) \right)_{t=0} = 0, \tag{19}$$

where $\rho = n_i - n_e$ is the scaled charge density. This equation will be referred to as the "reformulated Poisson equation".

Indeed, taking the difference of (7) and (9), we obtain the evolution equation of the current density $j = n_i u_i - n_e u_e$:

$$\partial_t j + \nabla(f_i - f_e) = -\left(n_i + \frac{n_e}{\varepsilon}\right)\nabla\phi. \tag{20}$$

From the difference of (6) and (8), we also get the continuity equation

$$\partial_t \rho + \nabla \cdot j = 0. \tag{21}$$

Then, taking the divergence of (20), the time derivative of (21), and combining these equations in order to eliminate the current, we obtain

$$\partial_{tt}^2 \rho - \nabla^2 : (f_i - f_e) = \nabla \cdot \left(\left(n_i + \frac{n_e}{\varepsilon}\right)\nabla\phi\right). \tag{22}$$

We remark that (22) is a consequence of system (6)–(9) whatever the way the potential ϕ is computed. Now, using the scaled Poisson equation (10), we can eliminate ρ in (22) and get (18).

Conversely, assuming (18) and using (22), we deduce that

$$\partial_{tt}^2(-\lambda^2\Delta\phi) = \partial_{tt}^2\rho. \tag{23}$$

Then, the initial conditions (19) allow to integrate (23) twice and find the Poisson equation.

In the quasineutral limit $\lambda \to 0$, the reformulated Eq. (18) formally converges toward the quasineutral potential equation (17). It does not degenerate into an algebraic equation like the Poisson equation does. Then, the reformulated two-fluid Euler–Poisson system (6)–(9) and (18) seems to be the appropriate framework to deal with problems which are partly or totally in the quasineutral regime.

The reformulated Poisson equation (18) is nothing but an harmonic oscillator equation for the electric charge with an appropriate forcing term. Indeed, for constant ion and electron densities, this equation yields

$$\partial_{tt}^2 \rho + \omega^2\left(n_i + \frac{n_e}{\epsilon}\right)\rho = \nabla^2 : (f_i - f_e). \tag{24}$$

The time discretization of this differential equation is a well-known subject. Indeed it is a common fact that an explicit discretization of this equation is conditionally stable while an implicit one is unconditionally stable. This is the idea behind the construction of the asymptotically stable scheme for the two-fluid Euler–Poisson system. In physical variables, Eq. (24) gives

$$\partial_{tt}^2 \rho + \left(\omega_{\mathrm{pi}}^2 + \omega_{\mathrm{pe}}^2\right)\rho = e\nabla^2 : \left(\frac{1}{m_i}\bar{f}_i - \frac{1}{m_e}\bar{f}_e\right), \tag{25}$$

where $\omega_{\mathrm{p}i}$ and $\omega_{\mathrm{p}e}$ are respectively the local ion and electron plasma frequencies: $\omega_{\mathrm{pi},e}^2 = \frac{e^2 n_{i,e}}{\varepsilon_0 m_{i,e}}$ with $n_{i,e}$ the local values of the ion and electron densities and where $\bar{f}_i$ and $\bar{f}_e$ are the momentum fluxes in physical variables, given by $\bar{f}_{i,e} = m_{i,e} n_{i,e} u_{i,e} \otimes u_{i,e} + p_{i,e}(n_{i,e})\mathrm{Id}$. In this form, it clearly appears that this harmonic oscillator equation monitors the plasma oscillations. Therefore, we have embedded the information about the plasma oscillations within the elliptic equation for the potential.

In the next section, we show how we can use this reformulated Poisson equation to derive asymptotic preserving time-stepping strategies for the Euler–Poisson problem.

3. An asymptotic preserving scheme for the two-fluid Euler–Poisson system

We first investigate time semi-discretizations of the two-fluid Euler–Poisson system. Indeed, the breakdown of the standard time-stepping strategies in the quasineutral regime is primarily a time stability problem. We defer the discussion of the space discretization to a forthcoming section.

3.1. Time discretization for the two-fluid Euler–Poisson system

3.1.1. The classical time discretization

We denote by Δt the time step, and by g^m an approximation of any function $x \mapsto g(x,t^m)$ with $t^m = m\Delta t$. The classical time discretization of the two-fluid Euler–Poisson system (6)–(10) consists of an implicit computation of the electric potential and an explicit computation of the hydro-fluxes such that:

$$\frac{n_{i,e}^{m+1} - n_{i,e}^m}{\Delta t} + \nabla \cdot q_{i,e}^m = 0, \tag{26}$$

$$\frac{q_i^{m+1} - q_i^m}{\Delta t} + \nabla f_i^m = -n_i^{m+1}\nabla\phi^{m+1}, \tag{27}$$

$$\frac{q_e^{m+1} - q_e^m}{\Delta t} + \nabla f_e^m = \frac{n_e^{m+1}}{\epsilon}\nabla\phi^{m+1}, \tag{28}$$

$$-\lambda^2\Delta\phi^{m+1} = n_i^{m+1} - n_e^{m+1}, \tag{29}$$

where $q_{i,e} = n_{i,e}u_{i,e}$ are the scaled fluid momenta.

In spite of being implicit in the source term, this scheme can be advanced like an explicit method. Indeed, assuming quantities known at time t^m, the densities are computed at time t^{m+1} using (26). Then (29) gives the potential ϕ^{m+1} and finally the momentum equations (27) and (28) are updated.

Like in the continuous case, we can derive a reformulation of the Poisson equation as follows (provided the Poisson equation is satisfied at time steps $m = 0$ and $m = 1$):

$$-\varepsilon\lambda^2\frac{(\Delta\phi^{m+1} - 2\Delta\phi^m + \Delta\phi^{m-1})}{\Delta t^2} - \nabla\cdot\left((\epsilon n_i^m + n_e^m)\nabla\phi^m\right) = \epsilon\nabla^2 : (f_i^{m-1} - f_e^{m-1}). \tag{30}$$

We remark that (30) is a time-explicit discretization of the reformulated Poisson equation (18). This scheme is known to be stable under the condition $\omega\Delta t \leqslant 1$ (where we recall that $\omega = (\lambda^2\varepsilon)^{-1}$ is the scaled plasma frequency) (see e.g. [27]). We do not prove (30) since the proof is similar to that of the corresponding formula for the (AP) scheme below.

3.1.2. An asymptotic preserving strategy

We now propose the following time-stepping strategy, which uses implicit mass fluxes but explicit momentum fluxes and implicit source terms:

$$\frac{n_{i,e}^{m+1} - n_{i,e}^m}{\Delta t} + \nabla \cdot q_{i,e}^{m+1} = 0, \tag{31}$$

$$\frac{q_i^{m+1} - q_i^m}{\Delta t} + \nabla f_i^m = -n_i^m\nabla\phi^{m+1}, \tag{32}$$

$$\frac{q_e^{m+1} - q_e^m}{\Delta t} + \nabla f_e^m = \frac{n_e^m}{\epsilon}\nabla\phi^{m+1}, \tag{33}$$

$$-\lambda^2\Delta\phi^{m+1} = n_i^{m+1} - n_e^{m+1}. \tag{34}$$

Here, the reformulation of the Poisson equation (which again is formally equivalent to the original Poisson equation provided the Poisson equation is satisfied at time steps $m = 0$ and $m = 1$) is as follows:

$$-\varepsilon\lambda^2\frac{(\Delta\phi^{m+1} - 2\Delta\phi^m + \Delta\phi^{m-1})}{\Delta t^2} - \nabla\cdot((\epsilon n_i^m + n_e^m)\nabla\phi^{m+1}) = \epsilon\nabla^2 : (f_i^m - f_e^m). \tag{35}$$

Now (35) corresponds to a time-implicit discretization of the reformulated Poisson equation (18).

We stress that the scheme (31)–(33) and (35) has the same cost as an explicit method. Indeed, (35) can also be written

$$-\frac{\varepsilon\lambda^2}{\Delta t^2}\Delta\phi^{m+1} - \nabla\cdot((\epsilon n_i^m + n_e^m)\nabla\phi^{m+1}) = \epsilon\nabla^2 : (f_i^m - f_e^m) + \frac{\varepsilon}{\Delta t^2}(2\rho^m - \rho^{m-1}), \tag{36}$$

where $\rho^m = n_i^m - n_e^m$ is the time discretization of the charge density. Eq. (36) appears as an elliptic problem which allows to compute ϕ^{m+1} provided that all quantities up to time step m are known. Then (32) and (33) allow to compute q_i^{m+1} and q_e^{m+1} in terms of known data and finally the densities are updated with (31).

The uniform stability property of this scheme for the linearized system is proved in a forthcoming article by the same authors in collaboration with Liu. More precisely, it is proven that its stability region is independent of the small parameter λ when $\lambda \to 0$. In the present work (see Section 4), this uniform stability is observed in the fully nonlinear case for one and two-dimensional test problems. Therefore, for an explicit method like numerical cost, a uniformly stable scheme for the Euler–Poisson system in the quasineutral limit is obtained.[2] When $\lambda \to 0$, the scheme converges to a scheme for the quasineutral limit, as it should, and as is apparent from (35).

At this point, a discussion of this method in view of the now classical direct implicit method [8,45] and implicit moment method [50,51] for PIC simulations is in order. We can rewrite Eq. (36) as

$$-\nabla\cdot((1+\chi^m)\nabla\phi^{m+1}) = \frac{\Delta t^2}{\lambda^2}\nabla^2 : (f_i^m - f_e^m) + \frac{1}{\lambda^2}(2\rho^{m+1} - \rho^m), \tag{37}$$

$$\chi^m = \frac{\Delta t^2}{\varepsilon\lambda^2}(\epsilon n_i^m + n_e^m), \tag{38}$$

where by analogy with the direct implicit method, we have introduced an "implicit susceptibility" χ^m. In the direct implicit method, the implicit susceptibility is computed from the particle discretization. Both (38) and the direct implicit expression of the susceptibility become much larger than unity when large time steps compared to the plasma period are used. However, the right-hand side of (37) involves the momentum fluxes, which do not appear in the direct implicit method and which makes it more similar, at this level, to the implicit moment method. In the latter, the momentum flux is computed from the particle distribution. However, the implicit moment method uses the electric field as the unknown for the field equations, by contrast to the present case where the equations are solved for the electric potential. Therefore the present method constitutes an alternative and has so far been developed in the fluid context. Its extension to kinetic models and particles methods is under current scrutiny.

The method is not fully implicit in the treatment of the electric field source term since the expression $n_{i,e}\nabla\phi$ is approximated by $n_{i,e}^m\nabla\phi^{m+1}$ at the right-hand sides of (32) and (33). A fully implicit treatment like e.g. $n_{i,e}^{m+1}\nabla\phi^{m+1}$ would make the susceptibility (38) depend on the densities at step $m+1$ and would prevent the reduction of the scheme to an explicit one. However, a higher level of implicitation can be performed without requiring a fully implicit treatment. Further investigations are planned for future work but our first series of tests seem to indicate that the partly implicit treatment of the source term is sufficient.

The present time-stepping strategy is only first order in time. The method can easily be extended to second order time-stepping strategies. In Section 4, we shall present preliminary results with the Lax–Wendroff scheme. The results show that the method performs well and is actually more accurate than the first order time-stepping strategy in smooth regions. However, the method develops instabilities at the plasma–vacuum transition, probably because of too small a numerical diffusion and further work is necessary to stabilize them. Other second order time-stepping strategies can also be investigated such as central schemes [54].

To be complete, we give a few words about how (35) is obtained. We proceed like in the continuous case. Eqs. (31)–(33) give respectively

$$\frac{\rho^{m+1} - \rho^m}{\Delta t} + \nabla\cdot j^{m+1} = 0 \tag{39}$$

and

$$\frac{j^{m+1} - j^m}{\Delta t} + \nabla(f_i^m - f_e^m) = -\nabla\cdot\left(\left(n_i^m + \frac{n_e^m}{\epsilon}\right)\nabla\phi^{m+1}\right). \tag{40}$$

[2] In a forthcoming work, we will present a variant of this scheme which is uniformly stable for *both* parameters λ and ε when they tend to zero.

Taking the discrete time derivative of (39), the divergence of (40) and combining the results gives

$$\frac{\rho^{m+1}-2\rho^m+\rho^{m-1}}{\Delta t^2}-\nabla^2:(f_i^m-f_e^m)=\nabla\cdot\left(\left(n_i^m+\frac{n_e^m}{\epsilon}\right)\nabla\phi^{m+1}\right). \tag{41}$$

Using Poisson's equation to eliminate the charge density at the l.h.s. of (41), we obtain (35). Reciprocally, starting from (35) and using that the Poisson equation is satisfied at time steps $m=0$ and $m=1$, we obtain Poisson equation (34).

3.2. Full discretization of the reformulated two-fluid Euler–Poisson system

In this section we propose full discretizations of the time semi-discretized systems (26)–(29) and (31)–(34). The space discretization uses the modified Lax–Friedrichs scheme [26,33]. Starting from this discretization, equivalent schemes corresponding to the reformulated two-fluid Euler–Poisson discretization are derived. The modified Lax–Friedrichs scheme is used in spite of its well-known large numerical diffusion because it involves discrete mass fluxes which are simple analytic functions of the momentum variables. This simplicity allows to pass from the discretization of the original Euler–Poisson system to that of the reformulated Euler–Poisson system. Generalizations to Godunov type solvers is actually in progress and we shall also present some preliminary results using Godunov based schemes in Section 4. However, additional work must be undertaken in order to explore the huge variety of available numerical schemes and to select the most suited ones to this new coupling methodology with the Poisson equation.

In this section we begin with the presentation of the classical discretization for the two-fluid Euler–Poisson system. Then we present the asymptotic preserving scheme. The schemes are presented in one space dimension for simplicity. The generalization to a multi-dimensional schemes is straightforward and is omitted.

We consider the domain $\Omega=(0,1)$ and we discretize it with a uniform mesh of step Δx given by $\Delta x=1/N$ where N is the number of cells. We set $x_{k+1/2}=k\Delta x$ for all $k=0,\ldots,N$. Let Δt be the time step, for all $m\geqslant 0$ we set $t^m=m\Delta t$ and we denote by $(U_{i,e})_k^m=((n_{i,e})_k^m,(q_{i,e})_k^m)$ and by ϕ_k^m the approximations of $((n_{i,e})(x,t),(q_{i,e})(x,t))$ and $\phi(x,t)$ for $x\in(x_{k-1/2},x_{k+1/2})$ and $t\in(t^m,t^{m+1})$, with $k=1,\ldots,N$ and $m\geqslant 0$. First, we recall the classical discretization.

3.2.1. Classical scheme for the two-fluid Euler–Poisson system

The full discretized equations associated to (26)–(29) using a modified Lax–Friedrichs solver is given by

$$\frac{(n_i)_k^{m+1}-(n_i)_k^m}{\Delta t}+\frac{1}{\Delta x}\left[\mathcal{Q}_i^m\left((U_i)_k^m,(U_i)_{k+1}^m\right)-\mathcal{Q}_i^m\left((U_i)_{k-1}^m,(U_i)_k^m\right)\right]=0, \tag{42}$$

$$\frac{(q_i)_k^{m+1}-(q_i)_k^m}{\Delta t}+\frac{F_i^m\left((U_i)_k^m,(U_i)_{k+1}^m\right)-F_i^m\left((U_i)_{k-1}^m,(U_i)_k^m\right)}{\Delta x}=-(n_i)_k^{m+1}\frac{\phi_{k+1}^{m+1}-\phi_{k-1}^{m+1}}{2\Delta x}, \tag{43}$$

for ions and

$$\frac{(n_e)_k^{m+1}-(n_e)_k^m}{\Delta t}+\frac{1}{\Delta x}\left[\mathcal{Q}_e^m\left((U_e)_k^m,(U_e)_{k+1}^m\right)-\mathcal{Q}_e^m\left((U_e)_{k-1}^m,(U_e)_k^m\right)\right]=0, \tag{44}$$

$$\frac{(q_e)_k^{m+1}-(q_e)_k^m}{\Delta t}+\frac{F_e^m((U_e)_k^m,(U_e)_{k+1}^m)-F_e^m\left((U_e)_{k-1}^m,(U_e)_k^m\right)}{\Delta x}=\frac{(n_e)_k^{m+1}}{\epsilon}\frac{\phi_{k+1}^{m+1}-\phi_{k-1}^{m+1}}{2\Delta x}, \tag{45}$$

for electrons, where the numerical fluxes are the following for $l=i$ or e:

$$\begin{aligned}\mathcal{Q}_l^m(U_g,U_d)&=\frac{q_g+q_d}{2}+\Lambda_l^m(n_g-n_d),\\ F_l^m(U_g,U_d)&=\frac{f_l(n_g,u_g)+f_l(n_d,u_d)}{2}+\Lambda_l^m(q_g-q_d).\end{aligned} \tag{46}$$

The fluxes $f_l(n,u)$ are given by (11). The upwind constants Λ_i^m and Λ_e^m, are chosen in order to ensure the consistency of the scheme (see [26]), we set:

$$\Lambda_l^m = \frac{1}{2}\max\left\{|(u_l)_k^m \pm \sqrt{p_l'((n_l)_k^m)/\epsilon_l}|; k = 1,\ldots,N\right\},$$

for $l = i$ or e with $\epsilon_i = 1$ and $\epsilon_e = \epsilon$.

The discrete potential ϕ_k^{m+1} is given by the classical discretized Poisson equation:

$$-\lambda^2\Delta_{ap}(\phi_k^{m+1}) := -\lambda^2\frac{\phi_{k+1}^{m+1} - 2\phi_k^{m+1} + \phi_{k-1}^{m+1}}{\Delta x^2} = (n_i)_k^{m+1} - (n_e)_k^{m+1}. \tag{47}$$

To ensure stability of the Lax–Friedrichs scheme in the absence of coupling with the Poisson equation, the time step must satisfy the CFL (Courant–Friedrichs–Levy) condition:

$$\Delta t \leqslant \frac{\Delta x}{\max(\Lambda_i^m, \Lambda_e^m)}. \tag{48}$$

When coupled with Poisson equation, the time step must additionally satisfy the constraint $\omega\Delta t \leqslant 1$, as shown in [27] (where we recall that $\omega = (\lambda\sqrt{\varepsilon})^{-1}$ is the electron plasma frequency).

The modified Lax–Friedrichs solver differs from the classical Lax–Friedrichs solver by the choice of the upwind constants. In the classical method, $\Lambda_i^m = \Lambda_e^m = \Delta x/(2\Delta t)$. Here, with two fluids, it is not possible to stabilize the classical method. Indeed, it is well known that in order to ensure the stability of the classical Lax–Friedrichs one must impose a CFL condition and an inverse CFL condition [26]. Here, for the stability of both the ion and electron Euler systems, we must set

$$C_{i,-}\frac{\Delta x}{\Lambda_i} \leqslant \Delta t \leqslant C_{i,+}\frac{\Delta x}{\Lambda_i} \quad \text{and} \quad C_{e,-}\frac{\Delta x}{\Lambda_e} \leqslant \Delta t \leqslant C_{e,+}\frac{\Delta x}{\Lambda_e},$$

where $C_{i,-}$, $C_{e,-}$, $C_{i,+}$ and $C_{e,+}$ are given positive constants. But, due to the small electron mass $\Lambda_e = \mathrm{O}(1/\sqrt{\epsilon}) \gg \Lambda_i = \mathrm{O}(1)$. Hence

$$C_{e,+}\frac{\Delta x}{\Lambda_e} < C_{i,-}\frac{\Delta x}{\Lambda_i},$$

and so it is not possible to find a time step satisfying both stability conditions.

Throughout the rest of the paper, the scheme (42)–(47) will be referred to as the classical scheme for the two-fluid Euler–Poisson system (C-EP). The scheme is semi-implicit since the electric force terms are implicit, but the resolution cost is the same as a fully explicit one, see Section 3.1.1. We note that taking explicit electric force terms would lead to an unstable discretization [27].

3.2.2. The asymptotic preserving scheme

The full discretization associated to (31)–(34) is given by

$$\frac{(n_i)_k^{m+1} - (n_i)_k^m}{\Delta t} + \frac{1}{\Delta x}\left[\mathcal{Q}_i^m\left((U_i)_k^{m+1/2}, (U_i)_{k+1}^{m+1/2}\right) - \mathcal{Q}_i^m\left((U_i)_{k-1}^{m+1/2}, (U_i)_k^{m+1/2}\right)\right] = 0, \tag{49}$$

$$\frac{(q_i)_k^{m+1} - (q_i)_k^m}{\Delta t} + \frac{F_i^m\left((U_i)_k^m, (U_i)_{k+1}^m\right) - F_i^m\left((U_i)_{k-1}^m, (U_i)_k^m\right)}{\Delta x} = -(n_i)_k^m\frac{\phi_{k+1}^{m+1} - \phi_{k-1}^{m+1}}{2\Delta x}, \tag{50}$$

$$\frac{(n_e)_k^{m+1} - (n_e)_k^m}{\Delta t} + \frac{1}{\Delta x}\left[\mathcal{Q}_e^m\left((U_e)_k^{m+1/2}, (U_e)_{k+1}^{m+1/2}\right) - \mathcal{Q}_e^m\left((U_e)_{k-1}^{m+1/2}, (U_e)_k^{m+1/2}\right)\right] = 0, \tag{51}$$

$$\frac{(q_e)_k^{m+1} - (q_e)_k^m}{\Delta t} + \frac{F_e^m((U_e)_k^m, (U_e)_{k+1}^m) - F_e^m\left((U_e)_{k-1}^m, (U_e)_k^m\right)}{\Delta x} = \frac{(n_e)_k^m}{\epsilon}\frac{\phi_{k+1}^{m+1} - \phi_{k-1}^{m+1}}{2\Delta x}, \tag{52}$$

with $U_{i,e}^{m+1/2} = ((n_{i,e})_k^m, (q_{i,e})_k^{m+1})$ and where the numerical fluxes $\mathcal{Q}_{i,e}^m$ and $F_{i,e}^m$ are given by (46). The discrete potential ϕ_k^{m+1} is still given by the classical discretized Poisson equation (47).

Like in the continuous case, for all $m \geqslant 2$, the discretized Poisson equation (47) is equivalent to

$$-\lambda^2\varepsilon\frac{\Delta_{ap}(\phi_k^{m+1}) - 2\Delta_{ap}(\phi_k^m) + \Delta_{ap}(\phi_k^{m-1})}{\Delta t^2} - \frac{1}{2\Delta x}\left((\epsilon n_i + n_e)_{k+1}^m\frac{\phi_{k+2}^{m+1} - \phi_k^{m+1}}{2\Delta x} - (\epsilon n_i + n_e)_{k-1}^m\frac{\phi_k^{m+1} - \phi_{k-2}^{m+1}}{2\Delta x}\right)$$
$$= \epsilon\frac{F_{k+3/2}^m - F_{k+1/2}^m - F_{k-1/2}^m + F_{k-3/2}^m}{2\Delta x^2} - \epsilon\frac{D_k^m - D_k^{m-1}}{\Delta t}, \tag{53}$$

provided that $F^m_{k+1/2} = F^m_i\left((U_i)^m_k, (U_i)^m_{k+1}\right) - F^m_e\left((U_e)^m_k, (U_e)^m_{k+1}\right)$, where

$$D^m_k = -\frac{\Lambda^m_i}{\Delta x}\left((n_i)^m_{k+1} - 2(n_i)^m_k + (n_i)^m_{k-1}\right) + \frac{\Lambda^m_e}{\Delta x}\left((n_e)^m_{k+1} - 2(n_e)^m_k + (n_e)^m_{k-1}\right), \tag{54}$$

and that the discrete Poisson equation (47) (with $m+1$ replaced by m) is satisfied at steps $m = 0$ and $m = 1$.

To prove this formula, we first remark that (49) can be rewritten

$$\frac{(n_i)^{m+1}_k - (n_i)^m_k}{\Delta t} + \frac{(q_i)^{m+1}_{k+1} - (q_i)^{m+1}_{k-1}}{2\Delta x} - \frac{\Lambda^m_i}{\Delta x}\left((n_i)^m_{k+1} - 2(n_i)^m_k + (n_i)^m_{k-1}\right) = 0.$$

The difference with the similar equation for electrons gives

$$\frac{\rho^{m+1}_k - \rho^m_k}{\Delta t} + \frac{j^{m+1}_{k+1} - j^{m+1}_{k-1}}{2\Delta x} + D^m_k = 0, \tag{55}$$

where we recall that $\rho = n_i - n_e$ and $j = n_i u_i - n_e u_e$ and where D^m_k is given by (54). The discrete time derivative of (55) yields

$$\frac{\rho^{m+1}_k - 2\rho^m_k + \rho^{m-1}_k}{\Delta t^2} + \frac{1}{\Delta t}\left(\frac{j^{m+1}_{k+1} - j^{m+1}_{k-1}}{2\Delta x} - \frac{j^m_{k+1} - j^m_{k-1}}{2\Delta x}\right) + \frac{D^m_k - D^{m-1}_k}{\Delta t} = 0. \tag{56}$$

From the momentum equations, we deduce

$$\frac{j^{m+1}_{k+1} - j^m_{k+1}}{\Delta t} + \frac{F^m_{k+3/2} - F^m_{k+1/2}}{\Delta x} = -\left((n_i)^m_{k+1} + \frac{(n_e)^m_{k+1}}{\epsilon}\right)\frac{\phi^{m+1}_{k+2} - \phi^{m+1}_k}{2\Delta x}.$$

Taking the discrete space derivative of this equation we obtain

$$\begin{aligned}
&\frac{1}{2\Delta x}\left(\frac{j^{m+1}_{k+1} - j^m_{k+1}}{\Delta t} - \frac{j^{m+1}_{k-1} - j^m_{k-1}}{\Delta t}\right) + \frac{1}{2\Delta x}\left(\frac{F^m_{k+3/2} - F^m_{k+1/2}}{\Delta x} - \frac{F^m_{k-1/2} - F^m_{k-3/2}}{\Delta x}\right)\\
&\quad = -\frac{1}{2\Delta x}\left(\left((n_i)^m_{k+1} + \frac{(n_e)^m_{k+1}}{\epsilon}\right)\frac{\phi^{m+1}_{k+2} - \phi^{m+1}_k}{2\Delta x} - \left((n_i)^m_{k-1} + \frac{(n_e)^m_{k-1}}{\epsilon}\right)\frac{\phi^{m+1}_k - \phi^{m+1}_{k-2}}{2\Delta x}\right).
\end{aligned}$$

Then, we combine this equation with (55) in order to eliminate the current, this gives

$$\begin{aligned}
&\frac{\rho^{m+1}_k - 2\rho^m_k + \rho^{m-1}_k}{\Delta t^2} + \frac{D^m_k - D^{m-1}_k}{\Delta t} - \frac{F^m_{k+3/2} - F^m_{k+1/2} - F^m_{k-1/2} + F^m_{k-3/2}}{2\Delta x^2}\\
&\quad = \frac{1}{2\Delta x}\left(\left((n_i)^m_{k+1} + \frac{(n_e)^m_{k+1}}{\epsilon}\right)\frac{\phi^{m+1}_{k+2} - \phi^{m+1}_k}{2\Delta x} - \left((n_i)^m_{k-1} + \frac{(n_e)^m_{k-1}}{\epsilon}\right)\frac{\phi^{m+1}_k - \phi^{m+1}_{k-2}}{2\Delta x}\right).
\end{aligned}$$

This equation is just a consequence of the discretized two-fluid Euler system (49)–(52) Now, like in the continuous case, using this result, we deduce the equivalence between the discrete Poisson equation (47) and the discrete reformulated Poisson equation (53) provided that (49)–(52) are satisfied and that the Poisson equation is satisfied at the two initial time steps. This concludes the proof of (53).

Throughout the rest of this paper, the scheme (49)–(53) will be referred to as the asymptotic preserving scheme for the two-fluid Euler–Poisson system (AP-EP). The first and second time iterations are performed with the classical scheme (C-EP) defined by (42)–(47). We stress again that this scheme can be solved with the cost of an explicit scheme and so, it induces no additional cost compared with the classical discretization (C-EP). Furthermore, the scheme (AP-EP) is expected to be asymptotically stable in the quasineutral limit since it provides an implicit discretization of the reformulated Poisson equation (18). This expected stability behavior is confirmed both by the analytical study (which will be published in a forthcoming work by the same authors in collaboration with Liu) and by the numerical results presented in the following section.

4. Numerical results: comparison between the classical and the asymptotic preserving schemes

In this section we perform numerical simulations in one space dimension for the two-fluid Euler–Poisson system. We present two test-cases and we compare the classical scheme, C-EP, defined by (42)–(47) and the

asymptotic preserving scheme, AP-EP, defined by (49)–(53). The first test-case is the perturbation of a uniform quasineutral stationary solution to two-fluid Euler–Poisson system. The second test-case models the expansion of a quasineutral plasma in the vacuum separating two electrodes.

4.1. Periodic perturbation of a stationary uniform quasineutral plasma

We consider the quasineutral uniform stationary solution W^0 of the two-fluid Euler–Poisson system given by $W^0 = (n_i^0 = 1, n_e^0 = 1, q_i^0 = 0, q_e^0 = 1, E^0 = 0)$ where we recall that $E = -\partial_x\phi$ is the electric field. The first test-case is the perturbation of this steady state. To this aim, we perform a simulation on the domain $(0,1)$ with periodic boundary conditions for the Euler systems and with homogeneous Dirichlet boundary conditions for the Poisson equation. Furthermore we consider the following initial condition which is a perturbation of W^0:

$$n_i(x,0) = n_e(x,0) = 1, \qquad q_i(x,0) = \delta\cos 2\pi x, \qquad q_e(x,0) = 1 + \delta\cos 2\pi x,$$

where $\delta = 10^{-2}$ is the perturbation amplitude. This test-case has already been studied in [13,15] where the solution of the linearized two-fluid Euler–Poisson system is given analytically. For small perturbations, this solution is close enough to the solution of the nonlinear system. We compare this analytical solution to the numerical solution computed by the classical scheme (C-EP) defined by (42)–(47) and the asymptotic preserving scheme (AP-EP) defined by (49)–(53).

We select parameters issued from plasma arc physics (see e.g. [6,2,4]) such that $c_i = c_e = 1$, $\gamma = 5/3$ and

$$\epsilon = 10^{-4}, \qquad \lambda = 10^{-4} \quad \left(\text{i.e. } \omega = \frac{1}{\lambda\sqrt{\epsilon}} = 10^6\right). \tag{57}$$

We initiate the AP-EP scheme with two iterations performed with the C-EP scheme following the conditions of the equivalence between the Poisson and reformulated Poisson equation as emphasized in Section 3.2.2. We summarize the conditions of the various simulations and the observed stability of the numerical solution in Table 1.

We note that it is not possible to simulate the case $\Delta t > \omega^{-1}$ and $\Delta x < \lambda$. Indeed, when the space step Δx is such that $\Delta x < \lambda$, then the condition $\Delta t < \omega^{-1}$ is necessarily satisfied thanks to the CFL condition (48). The small inertia of the electrons implies $|\Lambda_e| \gg |\Lambda_i|$ since $\Lambda_e \sim \mathrm{O}(1/\sqrt{\epsilon})$. This is sufficient to ensure that $\Delta t < \omega^{-1}$.

In Figs. 1–3 we present the results obtained with the classical scheme C-EP and with the asymptotic preserving scheme AP-EP. On these simulations, the time step and the space step satisfy $\Delta x = \lambda$ and $\Delta t < \omega^{-1}$. The presented quantities are the particle densities, the velocities and the electric potential. They are compared to the analytical values obtained with the linearized two-fluid Euler–Poisson model. The results are given at the scaled time $t = 0.1$. For both schemes the results are stable.

In Figs. 4–6 we present the same quantities when the space step does not respect anymore the condition $\Delta x \leqslant \lambda$ while the time step still satisfies $\Delta t < \omega^{-1}$. We observe that the schemes remain stable. It appears, comparing Figs. 2 and 11, that there is a difference with the analytical solution in the computation of the electron velocity amplitude and phase. This difference can be imputed to the bad consistency of the scheme for the electron velocity equation due to the mass ratio stiffness as $\epsilon = 10^{-4} \ll 1$. Indeed, when ϵ increases this lack of precision decreases as we can see in Fig. 7.

In Figs. 8–10 we present the results obtained with the classical scheme C-EP when *none* of the conditions $\Delta x \leqslant \lambda$ and $\Delta t < \omega^{-1}$ are satisfied. We note that after a very short time $t = 2 \times 10^{-4}$, the solution diverges for all variables. Then, the scheme C-EP is unstable for $\Delta t > \omega^{-1}$.

Table 1
Summary of the conditions of the various simulations and observed stability of the numerical solution

	$\Delta x = \lambda$, $\Delta t < \omega^{-1}$	$\Delta x > \lambda$, $\Delta t < \omega^{-1}$	$\Delta x > \lambda$, $\Delta t > \omega^{-1}$
C-EP	Figs. 1–3 – Stab.	Figs. 4–6 – Stab.	Figs. 8–10 – Unstab.
AP-EP	Figs. 1–3 – Stab.	Figs. 4–6 – Stab.	Figs. 11–13 – Stab.

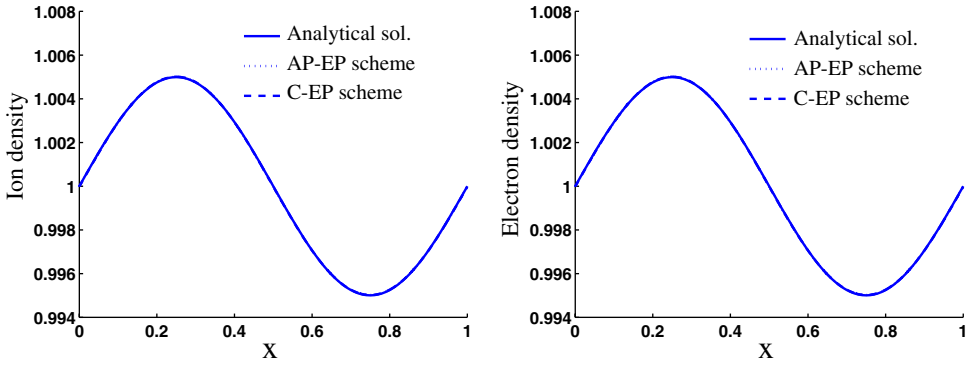

Fig. 1. Periodic perturbation test-case with $\Delta x = \lambda$ and $\Delta t < \omega^{-1}$, $\lambda = 10^{-4}$, $\epsilon = 10^{-4}$, $\omega = 10^{6}$. Ion density (left) and electron density (right): the classical scheme C-EP (dashed line) and the asymptotic preserving scheme AP-EP (dotted line) are compared to the analytical solution of the linearized two-fluid Euler–Poisson model (solid line) at the scaled time $t = 0.1$. All curves are identical.

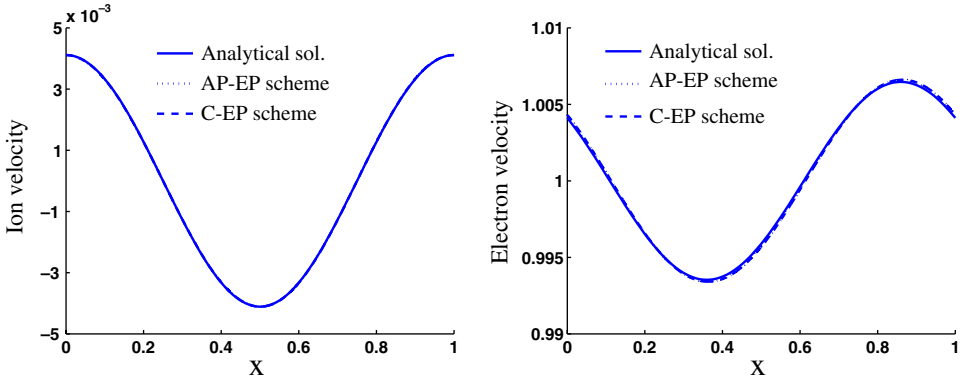

Fig. 2. Periodic perturbation test-case with $\Delta x = \lambda$ and $\Delta t < \omega^{-1}$, $\lambda = 10^{-4}$, $\epsilon = 10^{-4}$, $\omega = 10^{6}$. Ion velocity (left) and electron velocity (right): the classical scheme C-EP (dashed line) and the asymptotic preserving scheme AP-EP (dotted line) are compared to the analytical solution of the linearized two-fluid Euler–Poisson model (solid line) at the scaled time $t = 0.1$. On the right the C-EP and AP-EP curves are identical.

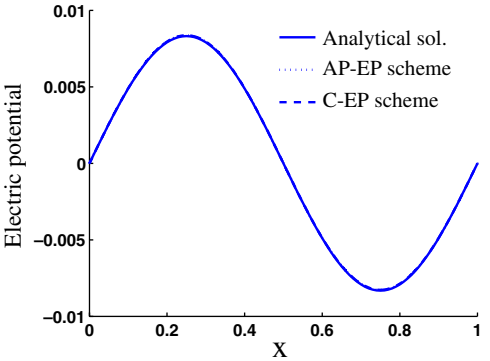

Fig. 3. Periodic perturbation test-case with $\Delta x = \lambda$ and $\Delta t < \omega^{-1}$, $\lambda = 10^{-4}$, $\epsilon = 10^{-4}$, $\omega = 10^{6}$. Electric potential: the classical scheme C-EP (dashed line) and the asymptotic preserving scheme AP-EP (dotted line) are compared to the analytical solution of the linearized two-fluid Euler–Poisson model (solid line) at the scaled time $t = 0.1$.

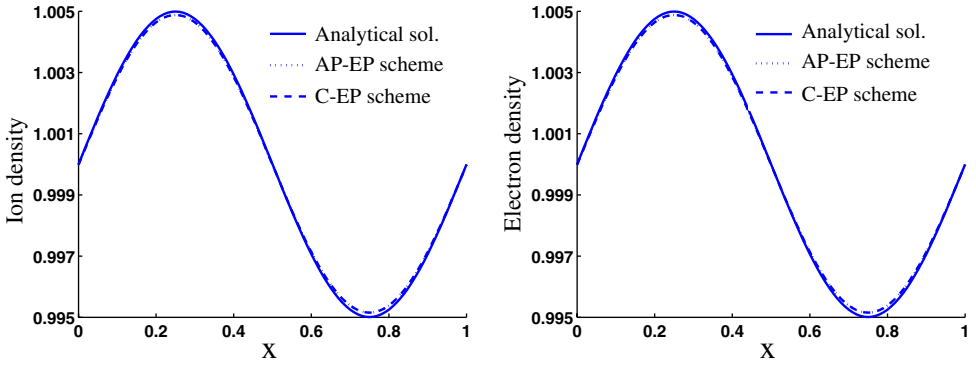

Fig. 4. Periodic perturbation test-case with $\Delta x = 10^{-2} > \lambda$ and $\Delta t < \omega^{-1}$, $\lambda = 10^{-4}$, $\epsilon = 10^{-4}$, $\omega = 10^{6}$. Ion density (left) and electron density (right): the classical scheme C-EP (dashed line) and the asymptotic preserving scheme AP-EP (dotted line) are compared to the analytical solution of the linearized two-fluid Euler–Poisson model (solid line) at the scaled time $t = 0.1$. In both figures, the curves "C-EP" and "AP-EP" are identical.

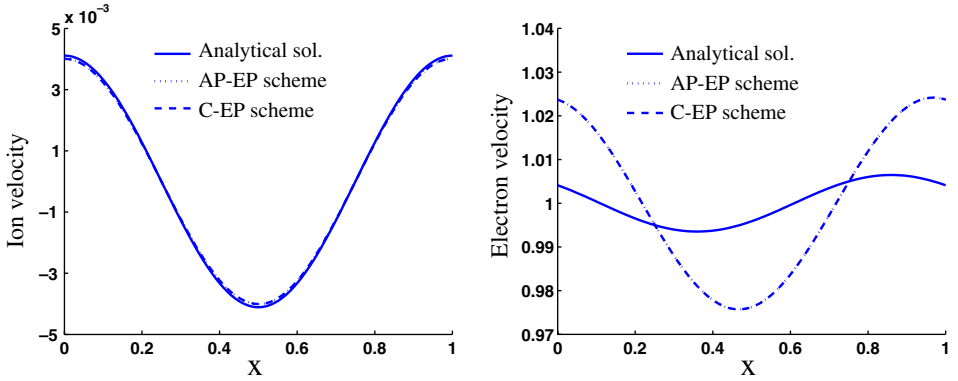

Fig. 5. Periodic perturbation test-case with $\Delta x = 10^{-2} > \lambda$ and $\Delta t < \omega^{-1}$, $\lambda = 10^{-4}$, $\epsilon = 10^{-4}$, $\omega = 10^{6}$. Ion velocity (left) and electron velocity (right): the classical scheme C-EP (dashed line) and the asymptotic preserving scheme AP-EP (dotted line) are compared to the analytical solution of the linearized two-fluid Euler–Poisson model (solid line) at the scaled time $t = 0.1$. In both figures, the curves "C-EP" and "AP-EP" are identical.

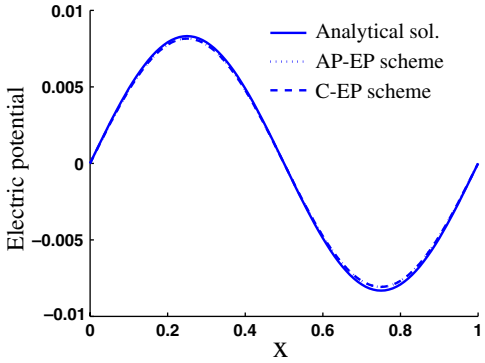

Fig. 6. Periodic perturbation test-case with $\Delta x = 10^{-2} > \lambda$ and $\Delta t < \omega^{-1}$, $\lambda = 10^{-4}$, $\epsilon = 10^{-4}$, $\omega = 10^{6}$. Electric potential: the classical scheme C-EP (dashed line) and the asymptotic preserving scheme AP-EP (dotted line) are compared to the analytical solution of the linearized two-fluid Euler–Poisson model (solid line) at the scaled time $t = 0.1$. The curves "C-EP" and "AP-EP" are identical.

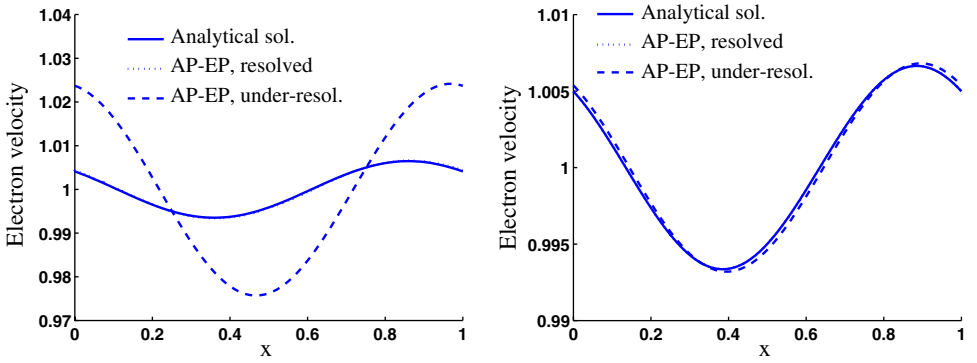

Fig. 7. Periodic perturbation test-case with $\lambda = 10^{-4}$ and $\omega = 10^4/\sqrt{\epsilon}$. Electron velocity at the scaled time $t = 0.1$ on the left for $\epsilon = 10^{-4}$ and on the right for $\epsilon = 10^{-1}$. Dotted line: the asymptotic preserving scheme AP-EP with $\Delta x = \lambda$ and $\Delta t < \omega^{-1}$ (both plasma frequency and Debye length are resolved). Dashed line: the AP-EP scheme with $\Delta x > \lambda$ and $\Delta t > \omega^{-1}$ (plasma frequency and Debye length are under-resolved). Solid line: analytical solution of the linearized problem. The curves "AP-EP, resolved" and "Analytical sol." are identical.

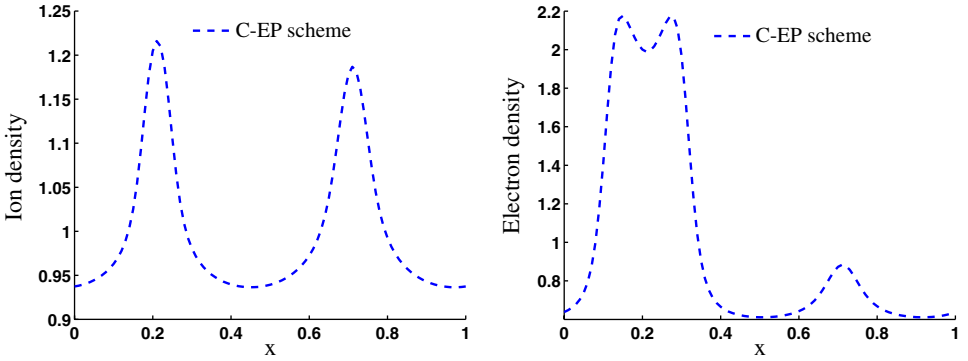

Fig. 8. Periodic perturbation test-case with $\Delta x = 10^{-2} > \lambda$ and $\Delta t > \omega^{-1}$, $\epsilon = 10^{-4}$, $\lambda = 10^{-4}$, $\omega = 10^6$. Ion density (left) and electron density (right) obtained with the classical scheme C-EP (dotted line) at the scaled time $t = 2 \times 10^{-4}$.

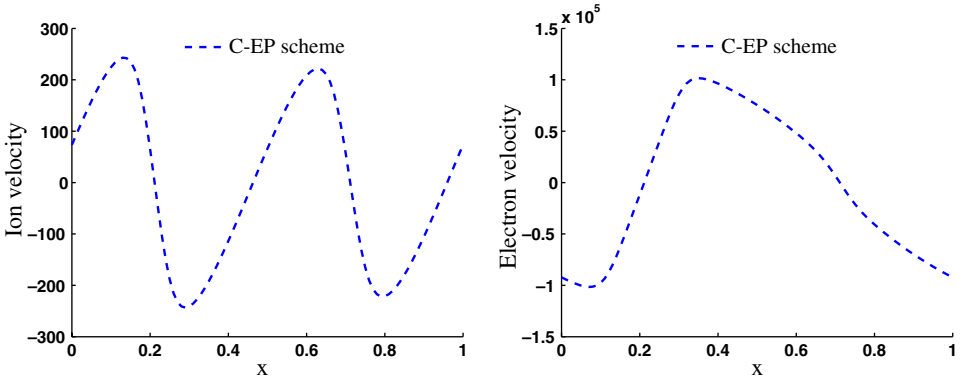

Fig. 9. Periodic perturbation test-case with $\Delta x = 10^{-2} > \lambda$ and $\Delta t > \omega^{-1}$, $\epsilon = 10^{-4}$, $\lambda = 10^{-4}$, $\omega = 10^6$. Ion velocity (left) and electron velocity (right) obtained with the classical scheme C-EP (dotted line) at the scaled time $t = 2 \times 10^{-4}$.

In Figs. 11–13 we compare the results obtained with the asymptotic preserving scheme AP-EP to the linearized analytical solution in the same condition i.e. when *none* of the conditions $\Delta x \leqslant \lambda$ and $\Delta t < \omega^{-1}$ are satisfied. We observe that the scheme is stable. The approximation for the electron velocity still suffers from a lack of precision mostly in the phase velocity.

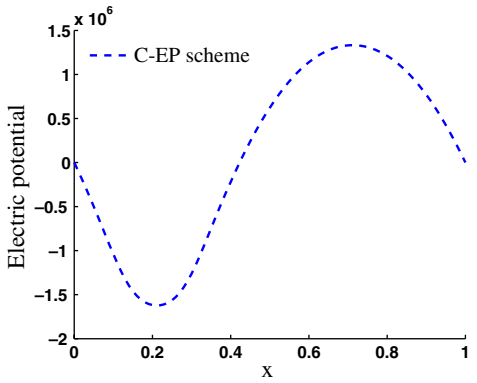

Fig. 10. Periodic perturbation test-case with $\Delta x = 10^{-2} > \lambda$ and $\Delta t > \omega^{-1}$, $\epsilon = 10^{-4}$, $\lambda = 10^{-4}$, $\omega = 10^6$. Electric potential obtained with the classical scheme C-EP (dotted line) at the scaled time $t = 2 \times 10^{-4}$.

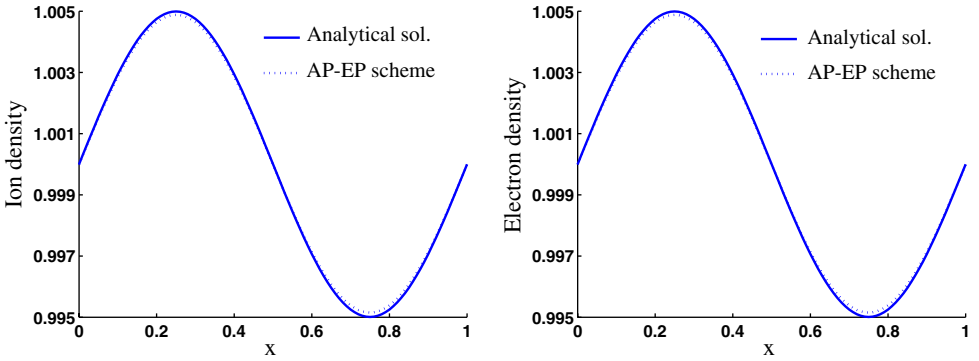

Fig. 11. Periodic perturbation test-case with $\Delta x = 10^{-2} > \lambda$ and $\Delta t > \omega^{-1}$, $\epsilon = 10^{-4}$, $\lambda = 10^{-4}$, $\omega = 10^6$. Ion density (left) and electron density (right): the asymptotic preserving scheme AP-EP (dotted line) is compared to the analytical solution of the linearized two-fluid Euler–Poisson model (solid line) at the scaled time $t = 0.1$.

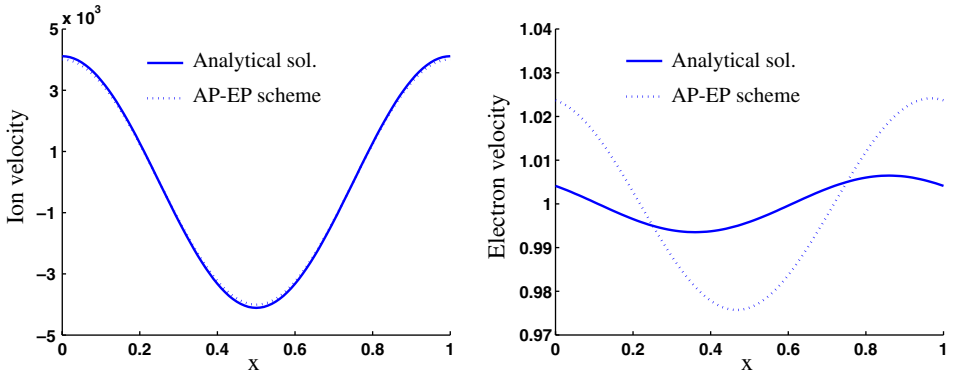

Fig. 12. Periodic perturbation test-case with $\Delta x = 10^{-2} > \lambda$ and $\Delta t > \omega^{-1}$, $\epsilon = 10^{-4}$, $\lambda = 10^{-4}$, $\omega = 10^6$. Ion velocity (left) and electron velocity (right): the asymptotic preserving scheme AP-EP (dotted line) is compared to the analytical solution of the linearized two-fluid Euler–Poisson model (solid line) at the scaled time $t = 0.1$.

Finally, in Fig. 14, we present results obtained with other solvers than Lax–Friedrichs scheme. We use the Lax–Wendroff scheme which is an order two scheme (see [33]) and the polynomial scheme which is a Riemann type solver (see [22,15]). They both give stable results when *none* of the conditions $\Delta x \leqslant \lambda$ and $\Delta t < \omega^{-1}$ are satisfied. Note that the error on the electron velocity is smaller for the order two Lax–Wendroff scheme.

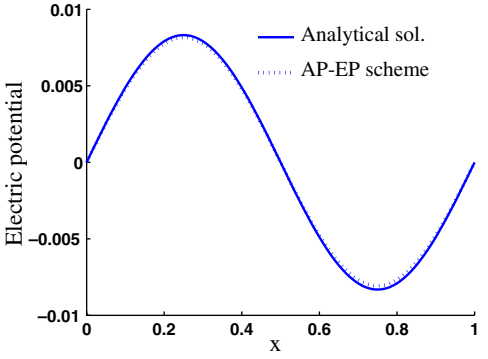

Fig. 13. Periodic perturbation test-case with $\Delta x = 10^{-2} > \lambda$ and $\Delta t > \omega^{-1}$, $\epsilon = 10^{-4}$, $\lambda = 10^{-4}$, $\omega = 10^6$. Electric potential: the asymptotic preserving scheme AP-EP (dotted line) is compared to the analytical solution of the linearized two-fluid Euler–Poisson model (solid line) at the scaled time $t = 0.1$.

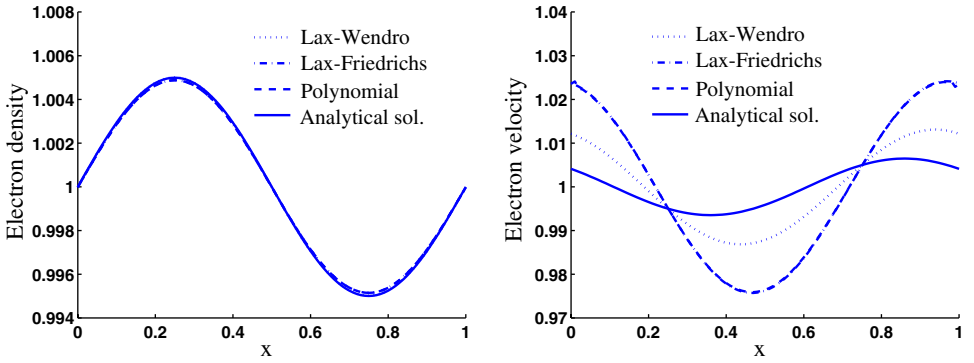

Fig. 14. Periodic perturbation test-case with $\Delta x = 10^{-2} > \lambda$ and $\Delta t > \omega^{-1}$, $\epsilon = 10^{-4}$, $\lambda = 10^{-4}$, $\omega = 10^6$. Electron density (left) and electron velocity (right): the asymptotic preserving scheme AP-EP with Lax–Wendroff solver (dotted line), polynomial solver (dashed line) and modified Lax–Friedrichs solver (dashed-dotted line) are compared to the analytical solution of the linearized two-fluid Euler–Poisson model (solid line) at the scaled time $t = 0.1$. On the left, the curves "Lax–Wendroff" and "Analytical sol." are identical. In both figures the curves "Lax–Friedrichs" and "Polynomial" are identical.

4.2. One-dimensional plasma expansion test-case

The second test-case we consider is that of a one-dimensional quasineutral plasma expansion in the vacuum separating two electrodes. At the beginning of the process, the domain is devoid of plasma. Then we set $n_i(x, t = 0) = n_e(x, t = 0) = 0$ for all $x \in (0, 1)$. The plasma is injected at the cathode $x = 0$, which is modeled by boundary conditions for two-fluid Euler system given as follows: $n_i(x = 0, t) = n_e(x = 0, t) = 1$ and $u_i(x = 0, t) = u_e(x = 0, t) = 1$, for all $t \geqslant 0$. Furthermore we set the following boundary conditions for the electric potential: $\phi(x = 0, t) = 0$ and $\phi(x = 1, t) = \phi_A$. We select parameters issued from plasma arc physics (see e.g. [2,4,6]) such that $c_i = c_e = 1$, $\gamma = 5/3$, $\epsilon = 10^{-4}$, $\lambda = 10^{-4}$ and $\phi_A = 10^2$. We recall that these parameters yield $\omega = 10^6$.

In Figs. 15–17, the ion and electron densities and velocities as well as the electric potential are displayed. The results are obtained with the classical and asymptotic preserving schemes C-EP and AP-EP at the scaled time $t = 0.09$. We simultaneously present the results obtained when $\Delta x = \lambda$ and $\Delta t < \omega^{-1}$ and when $\Delta x > \lambda$ and $\Delta t > \omega^{-1}$.

When $\Delta x = \lambda$, and $\Delta t < \omega^{-1}$, the results obtained with the different schemes are identical. When $\Delta x > \lambda$ and $\Delta t > \omega^{-1}$, the numerical results show clearly the instability of the classical scheme C-PE whereas the asymptotic preserving scheme AP-EP remains stable. We note that the AP-EP scheme suffers from a lack of precision

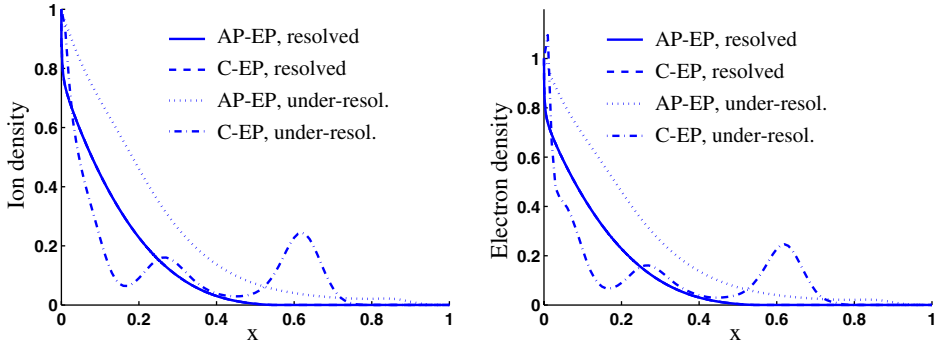

Fig. 15. Plasma expansion test-case for $\lambda = 10^{-4}$, $\epsilon = 10^{-4}$, $\omega = 10^6$ and $\phi_A = 100$. Ion density (left) and electron density (right) at the scaled time $t = 0.09$, in the case where the plasma frequency and Debye length are resolved (dashed line: C-EP scheme; solid line: AP-EP scheme) and under-resolved (dashed-dotted line: C-EP scheme; dotted line AP-EP scheme). The curves "C-EP, resolved" and "AP-EP, resolved" are identical.

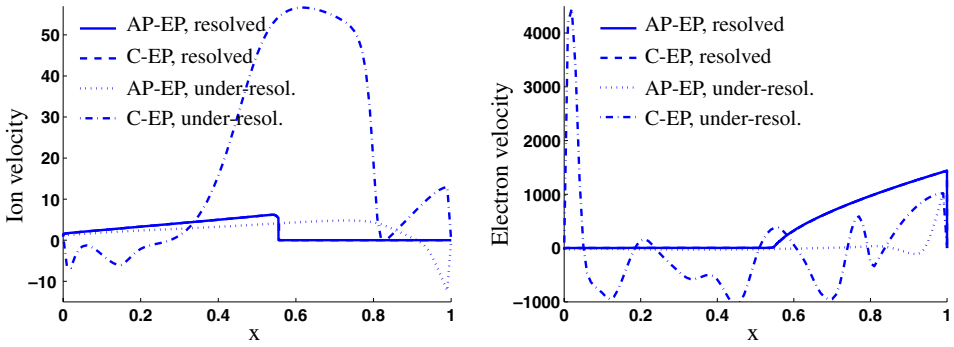

Fig. 16. Plasma expansion test-case for $\lambda = 10^{-4}$, $\epsilon = 10^{-4}$, $\omega = 10^6$ and $\phi_A = 100$. Ion velocity (left) and electron velocity (right) at the scaled time $t = 0.09$, in the case where the plasma frequency and Debye length are resolved (dashed line: C-EP scheme; solid line: AP-EP scheme) and under-resolved (dashed-dotted line: C-EP scheme; dotted line AP-EP scheme). The curves "C-EP, resolved" and "AP-EP, resolved" are identical.

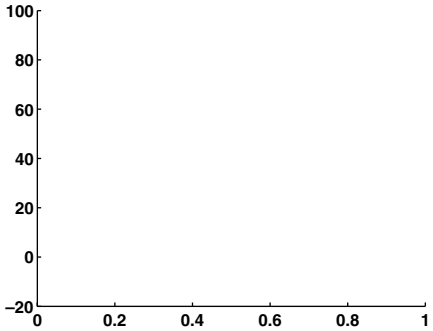

due to the use of a Lax–Friedrichs solver which is known to be very diffusive. The adaptation of the AP-EP method to Godunov type solver and (or) second order central solvers appears to be a necessity and is a work in progress.

4.3. Two-dimensional results for plasma expansion

We consider a square domain $\Omega = (0,1)\times(0,4)$ and we denote by Γ its boundary. At the beginning of the simulation the domain is devoid of plasma. Then,

$$n_i(t=0) = n_e(t=0) = 0.$$

We inject a quasineutral plasma on a part of Γ, such that:

$$(n_i)_{|\Gamma_{\text{inj}}} = (n_e)_{|\Gamma_{\text{inj}}} = \exp\left[-\left(\frac{y-2}{0.05}\right)^2\right], \tag{58}$$

$$(u_i)_{|\Gamma_{\text{inj}}} = (u_e)_{|\Gamma_{\text{inj}}} = 1, \tag{59}$$

where $\Gamma_{\text{inj}} = \{(x,y) \in \Gamma, x = 0, y \in [1.8, 2.2]\}$.

The boundary conditions for the electric potential are the following:

$$\phi(0,y,t) = 0, \quad \phi(1,y,t) = 100 \quad \text{and} \quad \partial_y\phi(x,0,t) = \partial_y\phi(x,4,t) = 0,$$

for all $y \in (0,4)$, all $x \in (0,1)$ and all $t > 0$.

Like in the one-dimensional test-cases the pressure laws are defined by $c_i = c_e = 1$ and $\gamma_i = \gamma_e = 5/3$ and the dimensionless parameters are given by $\lambda = 10^{-4}$ and $\epsilon = 10^{-4}$. This gives a scaled plasma frequency $\omega = 10^6$. Finally, the mesh is Cartesian with space steps $\Delta x = 1/100$ and $\Delta y = 1/100$.

The reformulated Poisson equation is implemented using a SPARSE matrix data structure compressed by row storage in order to minimize the memory and computation cost. From the open source library SPARSKIT [60], an iterative algorithm PGMRES preconditioned by an ILUT method (incomplete factorization LU with threshold and fill-in strategy) is used for the resolution of the system. Using an iterative method reduces the computational cost of the method as the final iterate of the previous time step can be used as the initial estimate for the next time step. Moreover it is not necessary to update the preconditioner at each time step.

The results are given in Figs. 18–23. Globally, they show that the scheme performs well in 2D, and confirms its stability for large time and space steps (compared to the Debye length and the electron plasma period). This kind of simulation would be extremely difficult to achieve with an explicit scheme, and would require considerable computer resources. However, we must notice that the physical validity of the simulation results depends on the accuracy of each fluid variables and in particular of the electron fluid velocity. We have seen that in one-dimensional simulations (see Section 4.1 and Figs. 5 and 7), this electron fluid velocity is not well described. It is important to note that this problem is already present in the classical scheme. Then it appears necessary to develop asymptotically stable schemes in both the quasineutral and small electron to ion mass ratio limits. This is work in progress (see Section 4.1 and Fig. 14).

In Fig. 18, we represent the ion and electron densities in log-scale at times $t = 0.005$, $t = 0.02$ and $t = 0.04$. The times $t = 0.005$, $t = 0.02$ are picked during the expansion phase of the plasma before it reaches the anode. The time $t = 0.04$ is roughly the time at which the plasma connects the two electrodes. To obtain these results, a two-dimensional version of the (AP) scheme with a modified Lax–Friedrichs solver has been used. Until the plasma connects the two electrodes at time $t = 0.04$, the gap is divided into a quasineutral plasma region and an electron beam region, like in the one-dimensional case. We remark that the electron beam has a fork shape, as it seems that the privileged location for electron emission lies on the sides of the plasma/beam interface. At the connection time $t = 0.04$, the electron beam does not exist anymore but the plasma density close to the anode is larger on the sides of the plasma bubble. These observations are confirmed by Fig. 21 where longitudinal and transversal sections of the density are represented.

In Fig. 19, we represent the ion and electron velocities at times $t = 0.005$, $t = 0.02$ and $t = 0.04$. During the expansion phase, the injected ions move towards the axis of symmetry of the device. For the electron, we remark an inversion of the velocity slightly upstream the boundary of the plasma. Inside the plasma, the x-component of the electron velocity is slightly negative which shows that the electrons move upstream. Downstream the plasma, in the electron beam part, the x-component of the electron velocity is of course positive and large. These observations are confirmed by the sectional views in Fig. 22.

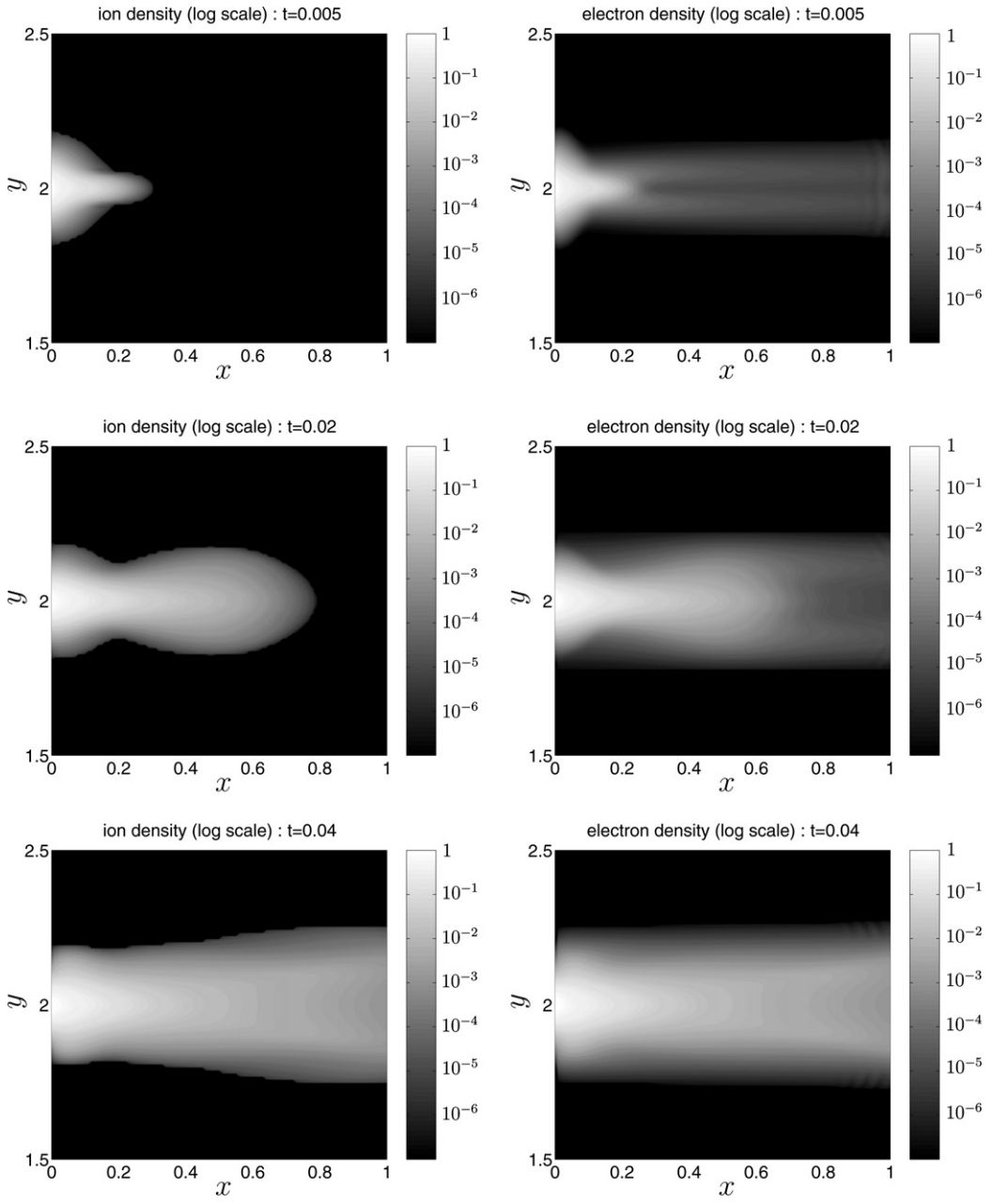

Fig. 18. Plasma expansion between two plane electrodes with $\epsilon = 10^{-4}$, $\lambda = 10^{-4}$ and $\omega = 10^{6}$. Ion density (left) and electron density (right) in log-scale at different times given by a two-dimensional (AP) scheme with the modified Lax–Friedrichs solver.

In Figs 20 and 23, we represent the electric potential at times $t = 0.005$, $t = 0.02$ and $t = 0.04$. During the expansion phase, we can distinguish three different regions. The first region is a cathode sheath located close to the cathode, where an important potential fall occurs. This phenomenon has been observed in 1D results and is due to the existence of a boundary layer of width equal to a few Debye lengths (see e.g. [15,20]). In particular, we notice oscillations of the potential near the cathode which do not disappear when time goes on. These oscillations, which have also been observed in one-dimensional simulations, are reduced when the mesh size is smaller. They are due to the fact that the mesh size is too large to correctly resolve this boundary layer.

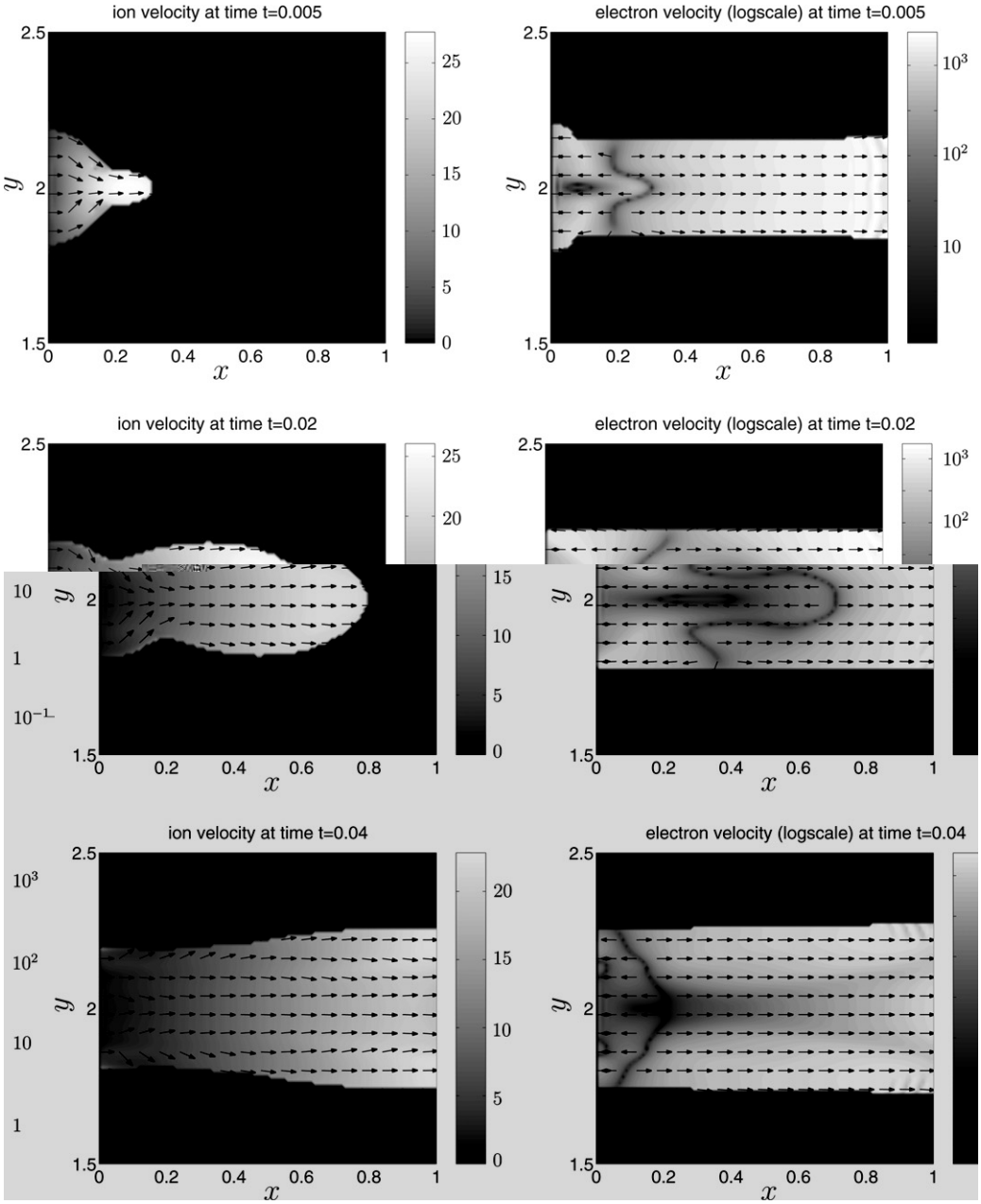

Fig. 19. Plasma expansion between two plane electrodes with $\epsilon = 10^{-4}$, $\lambda = 10^{-4}$ and $\omega = 10^{6}$. Ion velocity (left) and electron velocity (right) at different times by a two-dimensional (AP) scheme with the modified Lax–Friedrichs solver. Vector fields and field intensity are represented.

The second region is the plasma region inside which the potential is quite flat in the x direction and where we can observe negative barriers in the y direction during the expansion phase. The function of these barriers is to maintain the electrons inside the plasma and to prevent their leakage through the lateral boundaries of the plasma (see transversal sections in Fig. 23). By contrast, the lateral potential barriers become positive for times greater than the connection time. However, the physical relevance of these results after the connection time is questionable since no external circuit is taken into account. After the connection time, the plasma makes a highly conducting bridge between the two electrodes and the electric current consequently reaches

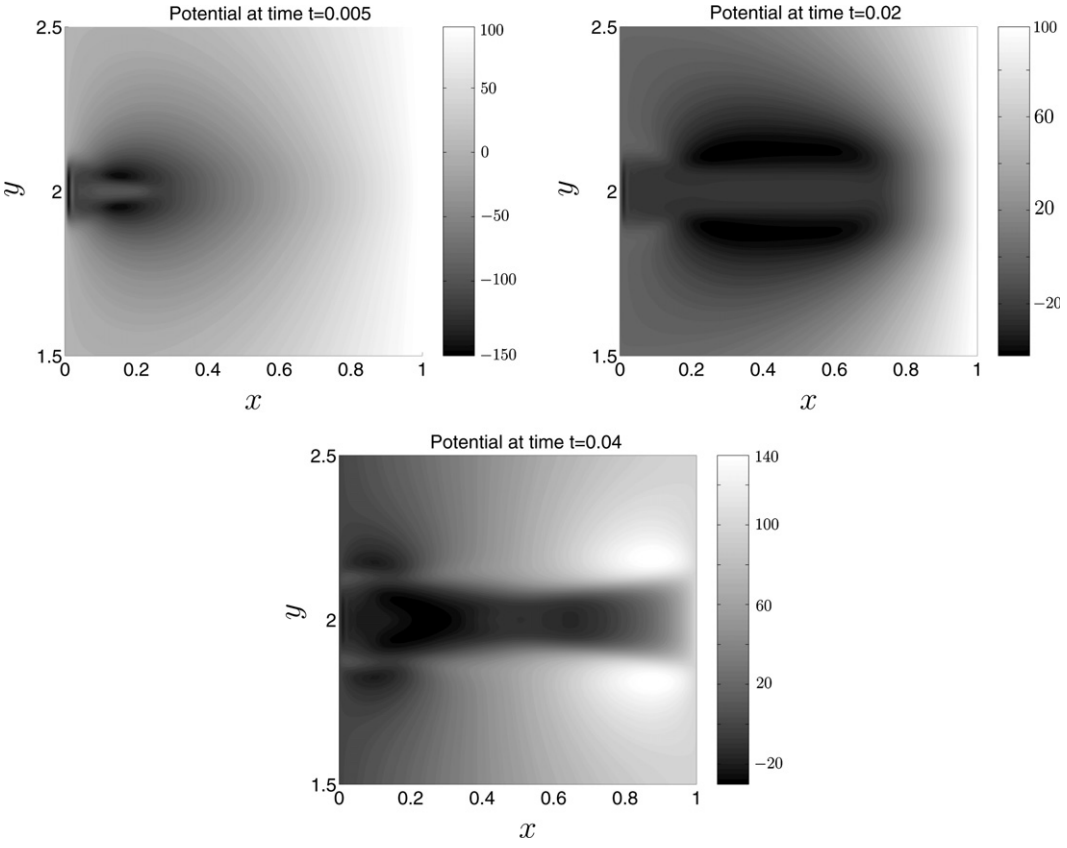

Fig. 20. Plasma expansion between two plane electrodes with $\epsilon = 10^{-4}$, $\lambda = 10^{-4}$ and $\omega = 10^{6}$. Electric potential at different times given by a two-dimensional (AP) scheme with the modified Lax–Friedrichs solver.

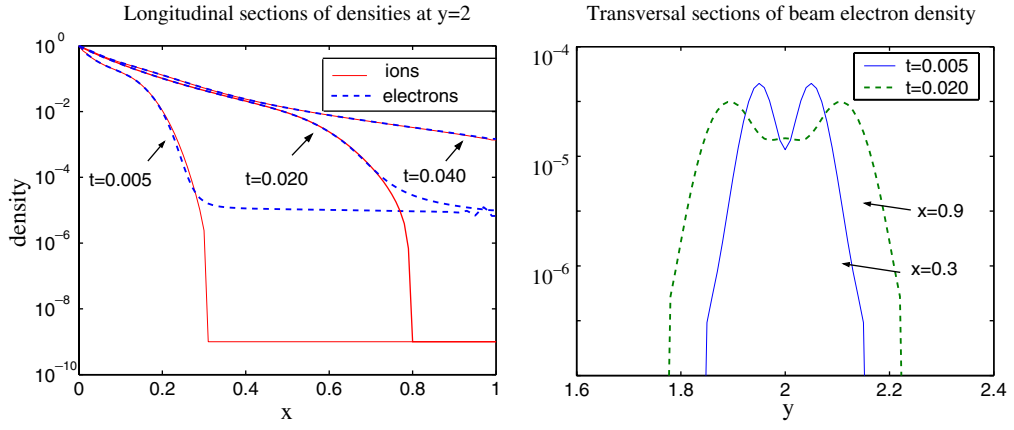

Fig. 21. Left: longitudinal sections of the densities along the symmetry axis $y = 2$ at times $t = 0.005$, $t = 0.020$ and $t = 0.040$. Right, transversal sections of the electron density in the beam at times $t = 0.005$ and $t = 0.020$.

very large values. In practice, the external circuit which produces the potential bias will react to this large current by reducing the bias. It is also likely that the plasma source is connected to the plasma and will stop delivering the plasma if the applied bias drops. In particular, if the plasma source is an ionization sheath, the electric field at the cathode may fall below the threshold for ionization in which case the plasma source

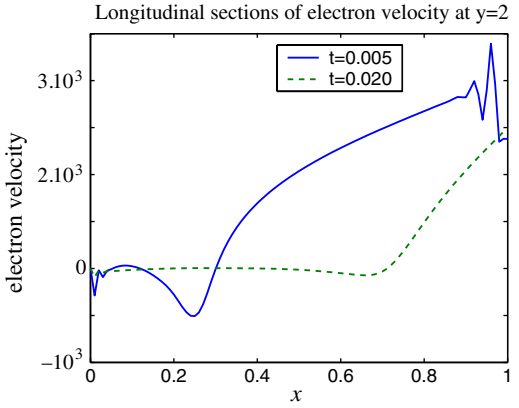

Fig. 22. Longitudinal sections of the electron velocity along the device axis $y = 2$ at times $t = 0.005$ and $t = 0.020$.

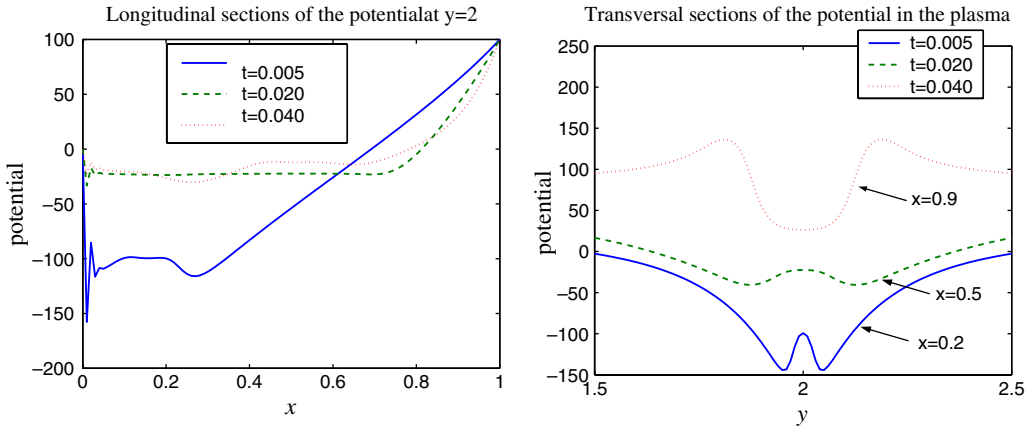

Fig. 23. Left: longitudinal sections of the potential along the symmetry axis $y = 2$ at times $t = 0.005$, $t = 0.020$ and $t = 0.040$. Right: transversal sections of the potential in the beam at times $t = 0.005$, $t = 0.020$ and $t = 0.040$.

extinguishes. In the present state, none of these phenomena has been taken into account. So, after the connection time, the dynamics is so intense that the physical relevance of the numerical results is questionable.

Finally, the third region concerns the expansion phase and corresponds to the beam zone where the potential grows from the plasma potential to the anode potential, as should be expected.

5. Conclusion

In this paper, we proposed an asymptotic preserving scheme in the quasineutral limit for the two-fluid Euler–Poisson system. This scheme has a comparable cost to that of an explicit discretization. The stability of the scheme in the quasineutral limit has been confirmed by numerical simulations in three different configurations. The first test-case is the perturbation of a uniform steady state in one space dimension. The other two test-cases concern the expansion of a plasma between two electrodes respectively in one and two space dimensions. We perform these simulation results with the modified Lax–Friedrichs solver in spite of its well-known diffusive behavior because the implementation of the asymptotic preserving strategy is easier in this case. But extensions to other solvers are being studied. In this paper, we have shown some preliminary results in the perturbation test-case for a Riemann solver based scheme (the polynomial scheme) and for the Lax–Wendroff scheme.

Following this idea, several works are in progress. First, we note that the scheme is still constrained by the CFL condition of the Euler systems. This constraint can be penalizing especially for electrons which have a very small mass. With the same methodology it is possible to bypass this limitation. In the same way, this idea can be applied to low Mach number limit of the compressible Euler equations. Finally extensions to other systems are under study. The application to the full Euler system including energy equations is straightforward. Finally, extensions to Drift-Diffusion models and to the Euler–Maxwell system have been designed and are currently under numerical development.

Acknowledgments

The authors thank D. Payan (CNES) and J.-F. Roussel (ONERA) for their support and encouragements. Support by the European network HYKE, funded by the EC as contract HPRN-CT-2002-00282, is also acknowledged.

References

[1] R. Abgrall, S. Karni, Computations of compressible multifluids, J. Comput. Phys. 169 (2001) 594.
[2] R.L. Boxman, P.J. Martin, D.M. Sanders (Eds.), Handbook of Vacuum Arcs Science and Technology, Fundamentals and Applications, Noyes Publications, Park Ridge, 1995.
[3] J.U. Brackbill, D.W. Forslund, An implicit method for electromagnetic plasma simulation in two dimensions, J. Comput. Phys. 46 (1982) 271.
[4] J.-P. Catani, D. Payan, Electrostatic behaviour of materials in a charging space environment, in: Proceedings of the 9th International Symposium on Materials in a Space Environment, 16–20 June 2003, Noordwijk, The Netherlands, ESA Publications Division, 2003, p. 3.
[5] F.F. ChenIntroduction to Plasma Physics and Controlled Fusion, vol. 1, Plenum Press, 1974.
[6] M. Cho, D.E. Hastings, Dielectric charging process and arcing rates of high voltage solar arrays, J. Spacecraft Rockets 28 (1990) 698.
[7] H.-H. Choe, N.S. Yoon, S.S. Kim, D.-I. Choi, A new unconditionally stable algorithm for steady-state fluid simulation of high density plasma discharge, J. Comput. Phys. 170 (2001) 550.
[8] B.I. Cohen, A.B. Langdon, A. Friedman, Implicit time integration for plasma simulation, J. Comput. Phys. 46 (1982) 15.
[9] Ph. Colella, M.R. Dorr, D.D. Wake, A conservative finite difference method for the numerical solution of plasma fluid equations, J. Comput. Phys. 149 (1999) 168.
[10] J.P. Collins, P. Colella, H.M. Glaz, An implicit–explicit Eulerian Godunov scheme for compressible flow, J. Comput. Phys. 116 (1995) 195.
[11] S. Cordier, E. Grenier, Quasineutral limit of Euler–Poisson system arising from plasma physics, Commun. Partial Differen. Equat. 25 (2000) 1099.
[12] S. Cordier, Y.-J. Peng, Système Euler–Poisson non linéaire. Existence globale de solutions faibles entropiques, RAIRO Modél. Math. Anal. Numér. 32 (1998) 1.
[13] P. Crispel, P. Degond, C. Parzani, M.-H. Vignal, Trois formulations d'un modéle de plasma quasi-neutre avec courant non-nul, C.R. Acad. Sci. Paris 338 (2004) 327.
[14] P. Crispel, P. Degond, M-H. Vignal, An asymptotically stable discretization for the Euler–Poisson system in the quasineutral limit, C.R. Acad. Sci. Paris, Ser. I 341 (2005) 323.
[15] P. Crispel, P. Degond, M.-H. Vignal, Quasi-neutral fluid models for current carrying plasmas, J. Comput. Phys. 205 (2005) 408.
[16] P. Degond, The Child–Langmuir law in the kinetic theory of charged-particles. Part 1, Electron flows in vacuum, in: B. Perthame (Ed.), Advances in Kinetic Theory, World Scientific, Singapore, 1994, p. 3.
[17] P. Degond, B. Lucquin-Desreux, Transport coefficients of plasmas and disparate mass binary gases, Trans. Theory Stat. Phys. 25 (1996) 595.
[18] P. Degond, C. Parzani, M.-H. Vignal, Un modéle d'expansion de plasma dans le vide, C.R. Acad. Sci. Paris Ser. I 335 (2002) 399.
[19] P. Degond, C. Parzani, M.-H. Vignal, A one-dimensional model of plasma expansion, Math. Comput. Modell. 38 (2003) 1093.
[20] P. Degond, C. Parzani, M.-H. Vignal, Plasma expansion in vacuum: modeling the breakdown of quasineutrality, SIAM Multiscale Model. Simul. 2 (2003) 158.
[21] P. Degond, C. Parzani, M.-H. Vignal, On plasma expansion in vacuum, in: Free Boundary Problems: Theory and Applications, in: P. Colli, C. Verdi, A. Visintin (Eds.), International Series of Numerical Mathematics, vol. 147, Birkhäuser Verlag, Basel, 2004, p. 103.
[22] P. Degond, P.-F. Peyrard, G. Russo, Ph. Villedieu, Polynomial upwind schemes for hyperbolic systems, C.R. Acad. Sci. Paris Ser. I 328 (1999) 479.
[23] P. Degond, P.-A. Raviart, An asymptotic analysis of the one-dimensional Vlasov Poisson system: the Child–Langmuir law, Asymptotic Anal. 4 (1991) 187.
[24] P. Degond, R. Talaalout, M.-H. Vignal, Electron transport and secondary emission in a surface of a solar cell, in: Proceedings of Multipactor, RF and DC corona and passive intermodulation in space RF hardware, ESTEC, Noordwijk, The Netherlands, 4–6 September 2000.

[25] G. DiPeso, D.W. Hewett, G.F. Simonson, Extension of the streamlined Darwin model to quasineutral plasmas, J. Comput. Phys. 111 (1994) 237.
[26] R. Eymard, T. Gallouët, R. Herbin, Finite volume methods, in: P.G. Ciarlet, J.L. Lions (Eds.), Handbook of Numerical Analysis, vol. VII, North-Holland, 2000, p. 713.
[27] Sylvie Fabre, Stability analysis of the Euler–Poisson equations, J. Comput. Phys. 101 (1992) 445.
[28] R.N. Franklin, J.R. Ockendon, Asymptotic matching of plasma and sheath in an active low pressure discharge, J. Plasma Phys. 4 (1970) 3521–3528.
[29] A. Friedman, S.E. Parker, S.L. Ray, C.K. Birdsall, Multi-scale particle-in-cell plasma simulation, J. Comput. Phys. 96 (1991) 54.
[30] Alex Friedman, Implicit multiscale PIC and related topics, in: Workshop on Multiscale Processes in Fusion Plasmas, IPAM, UCLA, 10–14 January 2005. Available from: <http://www.ipam.ucla.edu/publications/fus2005/fus2005_5425.pdf>.
[31] M.R. Gibbons, D.W. Hewett, The Darwin direct implicit particle-in-cell (DADIPIC) method for simulation of low frequency plasma phenomena, J. Comput. Phys. 120 (1995) 231.
[32] M.R. Gibbons, D.W. Hewett, Characterization of the Darwin direct implicit particle-in-cell method and resulting guidelines for operation, J. Comput. Phys. 130 (1997) 54.
[33] E. Godlewski, P.-A. Raviart, Numerical Approximation of Hyperbolic Systems of Conservation Laws, Springer, 1996.
[34] S.Y. Ha, M. Slemrod, Global existence of plasma ion sheaths and their dynamics, Commun. Math. Phys. 238 (2003) 149.
[35] D.W. Hewett, A.B. Langdon, Electromagnetic direct implicit plasma simulation, J. Comput. Phys. 72 (1987) 121.
[36] D.W. Hewett, C.W. Nielson, A multidimensional quasineutral plasma simulation model, J. Comput. Phys. 29 (1978) 219.
[37] S. Humphries Jr., Modeling ion extraction from a free-plasma surface with a flexible conformal mesh, J. Comput. Phys. 204 (2005) 587.
[38] S. Jin, Efficient asymptotic-preserving (AP) schemes for some multiscale kinetic equations, SIAM J. Sci. Comput. 21 (1999) 441.
[39] G. Joyce, M. Lampe, S.P. Slinker, W.M. Manheimer, Electrostatic particle-in-cell simulation technique for quasineutral plasma, J. Comput. Phys. 138 (1997) 540.
[40] H. Karimabadi, J. Driscoll, Y.A. Omelchenko, N. Omidi, A new asynchronous methodology for modeling of physical systems: breaking the curse of courant condition, J. Comput. Phys. 205 (2005) 755.
[41] R. Klein, Semi-implicit extension of a Godunov-type scheme based on low mach number asymptotics I: One-dimensional flow, J. Comput. Phys. 121 (1995) 213.
[42] D.A. Knoll, An improved convection scheme applied to recombining divertor plasma flows, J. Comput. Phys. 142 (1998) 473.
[43] N.A. Krall, A.W. Trivelpiece, Principles of Plasma Physics, San Francisco Press, 1986.
[44] A.B. Langdon, D.C. Barnes, Direct implicit plasma simulations, in: Multiple Time Scales, Academic Press, 1985.
[45] A.B. Langdon, B.I. Cohen, A. Friedman, Direct implicit large time-step particle simulation of plasmas, J. Comput. Phys. 51 (1983) 107.
[46] G. Lapenta, F. Iinoya, J.U. Brackbill, Particle-in-cell simulations of glow discharges in complex geometries, IEEE Trans. Plasma Sci. 23 (1995) 769.
[47] P.M. Lyster, J.-N. Leboeuf, A fluid-ion and particle–electron model for low-frequency plasma instabilities, J. Comput. Phys. 102 (1992) 180.
[48] A. Mankofsky, R.N. Sudan, J. Denavit, Hybrid simulation of ion beams in background plasma, J. Comput. Phys. 70 (1987) 89.
[49] P. Marcati, R. Natalini, Weak solutions to a hydrodynamic model for semiconductors: the Cauchy problem, Proc. Roy. Soc. Edinburgh Sec. A 125 (1995) 115.
[50] R.J. Mason, Implicit moment particle simulation of plasmas, J. Comput. Phys. 41 (1981) 233.
[51] R.J. Mason, Implicit moment PIC-hybrid simulation of collisional plasmas, J. Comput. Phys. 51 (1983) 484.
[52] R.J. Mason, Hybrid and collisional implicit plasma simulation models, in: Multiple Time Scales, Academic Press, 1985.
[53] R.J. Mason, An electromagnetic field algorithm for 2D implicit plasma simulation, J. Comput. Phys. 71 (1987) 429.
[54] H. Nessyahu, E. Tadmor, Non-oscillatory central differencing for hyperbolic conservation laws, J. Comput. Phys. 87 (1990) 408.
[55] S. Osher, R. Fedkiw, Level set methods: an overview and some recent results, J. Comput. Phys. 169 (2001) 463.
[56] F. Poupaud, M. Rascle, J.P. Vila, Global solutions to the isothermal Euler–Poisson system with arbitrary large data, J. Differen. Equat. 123 (1995) 93.
[57] P.W. Rambo, J. Denavit, Fluid and field algorithms for time-implicit plasma simulation, J. Comput. Phys. 92 (1991) 185.
[58] P.W. Rambo, J. Denavit, Time-implicit fluid simulation of collisional plasmas, J. Comput. Phys. 98 (1992) 317.
[59] P.W. Rambo, Finite-grid instability in quasineutral hybrid simulations, J. Comput. Phys. 118 (1995) 152.
[60] Y. Saad, Iterative Methods for Sparse Linear Systems, PWS Publishing, New York, 1996.
[61] R. Saurel, R. Abgrall, A mutiphase Godunov method for compressible multifluid and multiphase flows, J. Comput. Phys. 150 (1999) 425.
[62] R. Schneider, C.-D. Munz, The approximation of two-fluid plasma flow with explicit upwind schemes, Int. J. Numer. Model. 8 (2005) 399.
[63] J.A. Sethian, Level Set Methods. Evolving Interfaces in Geometry, Fluid Mechanic, Computer Vision, and Material Science, second ed., Cambridge University Press, 1999.
[64] U. Shumlak, J. Loverich, Approximate Riemann solver for the two-fluid plasma model, J. Comput. Phys. 187 (2003) 620.
[65] M. Slemrod, Shadowing and the plasma-sheath transition layer, J. Nonlinear Sci. 11 (2001) 193.
[66] M. Slemrod, The radio frequency driven plasma sheath: asymptotics and analysis, SIAM J. Appl. Math. 63 (2003) 1737.
[67] M. Slemrod, N. Sternberg, Quasi-neutral limit for Euler–Poisson system, J. Nonlinear Sci. 11 (2001) 193.

[68] N. Sternberg, V.A. Godyak, Solving the mathematical model of the electrode sheath in symmetrically driven RF discharges, J. Comput. Phys. 111 (1994) 347.
[69] H. Sze, J. Benford, W. Woo, B. Harteneck, Dynamics of a virtual cathode oscillator driven by a pinched diode, Phys. Fluids 29 (1986) 3873.
[70] S.O. Unverdi, G. Tryggvason, A front-tracking method for viscous, incompressible, multi-fluid flows, J. Comput. Phys. 100 (1992) 25.
[71] P.L.G. Ventzek, T.J. Sommerer, R.J. Hoekstra, M.J. Kushner, Two-dimensional hybrid model of inductively coupled plasma sources for etching, Appl. Phys. Lett. 63 (1993) 605.
[72] P.L.G. Ventzek, R.J. Hoekstra, M.J. Kushner, Two-dimensional modeling of high plasma density inductively coupled sources for materials processing, J. Vac. Sci. Technol. B 12 (1994) 461.
[73] J.M. Wallace, J.U. Brackbill, D.W. Forslund, An implicit moment electromagnetic plasma simulation in cylindrical coordinates, J. Comput. Phys. 63 (1986) 434.
[74] S. Wang, Quasineutral limit of Euler–Poisson system with and without viscosity, Commun. Partial Differential Equations 29 (2004) 419.
[75] T. Westermann, Particle-in-cell simulations with moving boundaries – adaptive mesh generation, J. Comput. Phys. 114 (1994) 161.
[76] H.C. Yee, R.F. Warming, A. Harten, Implicit total variation diminishing (TVD) schemes for steady-state calculations, J. Comput. Phys. 57 (1985) 327.
[77] H.C. Yee, Explicit and implicit multidimensional compact high-resolution shock-capturing methods: formulation, J. Comput. Phys. 131 (1997) 216.
[78] D.L. Youngs, Time-dependent multi-material flow with large fluid distortion, in: K.W. Morton, M.J. Baines (Eds.), Numerical Methods for Fluid Dynamics, Academic Press, New York, 1982, p. 273.